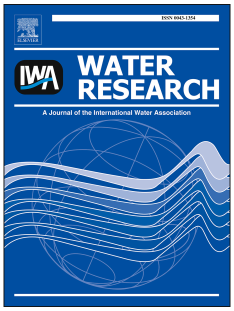

Removal of atrazine and its by-products from water using electrochemical advanced oxidation processes

Simon Komtchou, Ahmad Dirany, Patrick Drogui, Didier Robert, Pierre Lafrance

PII: S0043-1354(17)30698-X
DOI: 10.1016/j.watres.2017.08.036
Reference: WR 13159

To appear in: *Water Research*

Received Date: 25 May 2017
Revised Date: 8 August 2017
Accepted Date: 15 August 2017

Please cite this article as: Komtchou, S., Dirany, A., Drogui, P., Robert, D., Lafrance, P., Removal of atrazine and its by-products from water using electrochemical advanced oxidation processes, *Water Research* (2017), doi: 10.1016/j.watres.2017.08.036.

GRAPHICAL ABSTRACT

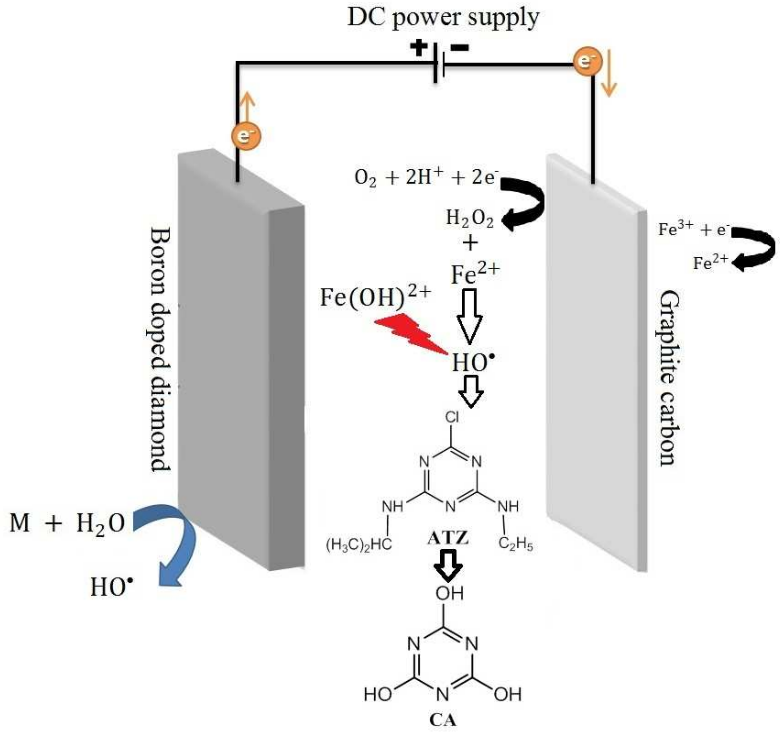

REMOVAL OF ATRAZINE AND ITS BY-PRODUCTS FROM WATER USING ELECTROCHEMICAL ADVANCED OXIDATION PROCESSES

Simon Komtchou [1], Ahmad Dirany [2], Patrick Drogui[*3], Didier Robert [4], Pierre Lafrance [5]

[1] Ph.D. student, Institut National de la Recherche Scientifique (INRS-Centre Eau, Terre et Environnement, Université du Québec, 490 rue de la Couronne, Québec, Qc, Canada, G1K 9A9, Phone : (418) 654-4478, Fax : (418) 654-2600, email : simon.komtchou@ete.inrs.ca

[2] Research associate, Institut National de la Recherche Scientifique (INRS-Centre Eau, Terre et Environnement), Université du Québec, 490 rue de la Couronne, Québec, Qc, Canada, G1K 9A9, Phone : (418) 654-2550, Fax : (418) 654-2600, email : ahmad.dirany@ete.inrs.ca

[3] Professor, Institut National de la Recherche Scientifique (INRS-Centre Eau, Terre et Environnement), Université du Québec, 490 rue de la Couronne, Québec, Qc, Canada, G1K 9A9, Phone : (418) 654-3119, Fax : (418) 654-2600, email : patrick.drogui@ete.inrs.ca

[4] Professor, Institut de Chimie et Procédés pour l'Énergie, l'Environnement et la Santé (ICPEES), CNRS, Université de Strasbourg, rue Victor Demange, 57500 Saint-Avold, France, Phone : (33) 3 87 93 91 85, email : d.robert@unistra.fr

[5] Professor, Institut National de la Recherche Scientifique (INRS-Centre Eau, Terre et Environnement), Université du Québec, 490 rue de la Couronne, Québec, Qc, Canada, G1K 9A9, Phone : (418) 654-2543, Fax : (418) 654-2600, email : pierre.lafrance@ete.inrs.ca

Paper submitted to be published in Water Research

* Corresponding author :
E-mail: patrick.drogui@ete.inrs.ca
Tel: (418) 654 3119; Fax: (418) 654 2600

May, 2017

ABSTRACT

Atrazine (ATZ) is one of the most common pesticides detected in surface water in Quebec (Canada). The present study was mainly focused on the degradation of ATZ and its by-products using electrochemical advanced oxidation processes such as photo-electro-Fenton (PEF), electro-Fenton (EF) and anodic-oxidation with simultaneous H_2O_2 formation (AO - H_2O_2). The comparison of these processes showed that PEF process was found to be the most effective process in removing ATZ and its by-products from both synthetic solution (ATZ_0 = 100 µg L^{-1}) and real agricultural surface water enriched with ATZ (ATZ_0 = 10 µg L^{-1}). Different operating parameters, including wavelength of the light, pH, current density and the presence of natural organic matter (humic acids) were investigated for PEF process using boron-doped diamond (BDD) anode and graphite cathode. The current density and the wavelength of the light were the most important parameters in the ATZ degradation efficiency. The best operating conditions were recorded for the synthetic samples at a current density of 18.2 mA cm^{-2}, a pH of 3.0 and treatment time of 45 min. Results showed that atrazine-desethyl-desisopropyl (DEDIA) was the most important by-product recorded. More than 99% of ATZ oxidation was recorded after 15 min of treatment and all the concentrations of major by-products were less than the limit of detection after 45 min of treatment. The PEF process was also tested for real surface water contaminated by ATZ: i) with and without addition of iron; ii) without pH adjustment (pH ~ 6.7) and with pH adjustment (pH ~3.1). In spite of the presence of radical scavenger and iron complexation the PEF process was more effective to remove ATZ from real surface water when the pH value was adjusted near to 3.0. The ATZ removal was 96.0% with 0.01 mM of iron (k_{app} = 0.13 min^{-1}) and 100% with 0.1 mM of iron (k_{app} = 0.17 min^{-1}).

Keywords: Atrazine; Degradation, Photoelectro-Fenton; Hydroxyl radicals; Energy consumption

.

Highlights

- PEF process is a feasible technology for the treatment of water contaminated by ATZ.
- More than 99% of ATZ oxidation was recorded after 15 min of treatment in synthetic effluent.
- Atrazine-desethyl-desisopropyl (DEDIA) was the most important by-product recorded.
- 100% of ATZ was removed from surface water in spite of the presence of radical scavengers.

1. INTRODUCTION

Pesticides represent an effective solution to increase food production, ensure the maintenance of railways, gardens and golf courses. Since two decades, the market of sales and the world consumption of pesticides continually increased (Drogui and Lafrance 2012). Among herbicides, atrazine has received much attention in the past and in recent years. Atrazine (ATZ) was used mainly to fight weed and grass weeds which harm the culture of corn, sorghum and sugarcane (Solomon et al. 1996). In Quebec (Canada), as well as in other countries such as USA and Spain, atrazine is one of the most common pesticides detected in the surface water and groundwater (Hildebrandt et al. 2008, Giroux et al. 2010, Reilly et al. 2012, Giroux and Pelletier 2012). The presence of atrazine in aquatic ecosystems have negative impacts on the phytoplankton species which contribute significantly to the primary production (DeLorenzo et al. 2001); on the larval amphibians such as northern leopard frog (Koprivnikar 2010) and on the neonatal turtles (Neuman-Lee and Janzen 2011). Moreover, scientific reports found that atrazine can act as an endocrine disruptor (Trentacoste et al. 2001) who induces complete feminization of amphibians such as *Xenopus laevis* (Hayes et al. 2010). Considering the toxicity of ATZ on aquatics species and the risk to human health, many research efforts attempted to eliminate this herbicide from aquatic environment with efficient treatment technology such as advanced oxidation processes (AOPs). The AOPs are environmentally friendly chemical, photochemical, photocatalytic, electrochemical and photoelectrochemical technologies based on the production of hydroxyl radical ($HO^\bullet$) (Komtchou et al. 2016a). In wastewater treatment, hydroxyl radical have a strong oxidizing power ($E°$ ($HO^\bullet/H_2O$) = 2.80 V *vs.* standard hydrogen electrode (SHE) which can react with organic compounds and their by-products degradation, until mineralization into CO_2, water and inorganic ions. Among these AOPs methods, the electrochemical advanced oxidation processes (EAOPs) such as anodic oxidation with electrogenerated H_2O_2 (AO - H_2O_2), electro-Fenton (EF) and photoelectro-Fenton (PEF) have been successfully applied to degrade and mineralize ATZ in water effluents (Borràs et al. 2010, Oturan et al. 2012, Ding et al. 2017, Aquino et al. 2017). Unfortunately, none of these studies have tracking the evolution of by-products of ATZ during the different steps of degradation. Therefore, this study investigates the EAOPs using boron-doped diamond (BDD) anode and graphite cathode to remove atrazine and its by-products from surface water by means of undivided electrochemical cell. The choice of BDD over conventional electrodes (PbO_2, SnO_2, Ti/IrO_2) can be justified by the high quality and properties of this electrode such as stability to corrosion and inert surface with low adsorption properties (Panizza and Cerisola 2009). Likewise, the choice to use graphite plate as cathode is justified by its efficiency to generate the H_2O_2 (Eq. (1)) by cathodic reduction of dissolved oxygen (Khataee et al. 2012, Komtchou et al. 2016b).

$$O_2\,(g) + 2H^+ + 2e^- \rightarrow H_2O_2 \qquad (1)$$

In the AO-H_2O_2 process, hydroxyl radicals are generated on the anode surface (M) from the oxidation of water (Eq. (2)) when the current intensity is applied. The principal mechanism of pesticide degradation is direct oxidation at the anode surface.

$$M + H_2O \rightarrow M\,(HO^\bullet) + H^+ + e^- \qquad (2)$$

Moreover, when the graphite plate is used as cathode electrode, the electrochemical reduction of dissolved O_2 at the cathode surface produces H_2O_2. It is possible that the decomposition of H_2O_2 gives other weaker oxidant such as hydroperoxyl radical (Eq. (3)) that can participate to the degradation of pesticides.

$$H_2O_2 \rightarrow HO_2^\bullet + H^+ + e^- \qquad (3)$$

In the EF process, the highly oxidizing $HO^\bullet$ is produced via Fenton's reaction in acidic medium (Eq. (4)) when the electrogenerated H_2O_2 reacts with iron catalyst (Fe^{2+}) added in the solution.

The cathode ensures to continuously generate Fenton's reagents (Eqs. (1) and (5)). Likewise, the efficiency of EF can be improved under UV irradiation during electrolysis.

$$H_2O_2 + Fe^{2+} \rightarrow Fe^{3+} + HO^{\bullet} + OH^{-} \quad (4)$$

$$Fe^{3+} + e^{-} \rightarrow Fe^{2+} \quad (5)$$

In the PEF process, the treated solution under EF conditions is simultaneously irradiated with UV light and the photolysis of $Fe(OH)^{2+}$ contribute to generates a greater amount of $HO^{\bullet}$ (Eq. (6)). Likewise, the regeneration of Fe^{2+} improves the Fenton's reaction for $HO^{\bullet}$ formation (Eq. (4)).

$$Fe(OH)^{2+} + h\nu \rightarrow HO^{\bullet} + Fe^{2+} \quad (6)$$

According to Irmak et al. (2006) and Masomboon et al. (2010), the other advantage of PEF is the photodecarboxylation of iron complexes that generates carbon dioxide and ferrous iron (Eq. (7)).

$$Fe(OOCR)^{2+} + h\nu \rightarrow Fe^{2+} + CO_2 + R^{\bullet} \quad (7)$$

The combination of electrochemical, photochemical and photo-electrochemical processes in a same reactor gives an advantage to the PEF process to remove from water ATZ and its by-products. Some authors argued that PEF process can be effectively used to remove high concentrations of ATZ (*e.g.* 20 and 30 mg L^{-1}) in a small volume of synthetic solution (Borràs et al. 2010, Garza-Campos et al. 2014, Ding et al. 2017). Nowadays, the challenge is to develop industrial low-cost technologies to treat a large volume of real water and capable of simultaneously removing micro-pollutants (such as pesticides) and their metabolites that can be more toxic than the original compounds.

The aim of this paper is to show the efficiency of a novel photo-electro-Fenton (PEF) process to remove relatively low concentrations of ATZ (10 and 100 µg L^{-1}) from water, in comparison with other electrochemical advanced oxidation processes such as electro-Fenton (EF) and anodic-oxidation with simultaneous H_2O_2 formation (AO - H_2O_2). The experiments were carried out using a semi-pilot reactor having 5 L of capacity. The effects of operating parameters such as wavelength lights and current density were studied. Likewise, the effect of natural dissolved organic matter (humic acids) and the values of initial pH were investigated. The effectiveness of PEF process to remove ATZ from real agricultural surface water enriched with ATZ was also investigated.

2. MATERIALS AND METHODS

2.1. Preparation of the synthetic solution of atrazine

ATZ and five of its by-products (ATZ-OH, DEA, DIA, DEDIA and CA) were purchased from Sigma Aldrich (Oakville, ON, Canada) in the highest purity: 99.9%. ATZ stock solution (10 mg L^{-1}) was prepared each week in 1000 mL of deionized water (conductivity = 0.31 µs cm^{-1}). Dissolution of atrazine was carried out in the darkness. Mixing was achieved by a teflon-covered stirring bar installed in the bottom of the beaker at the room temperature (23 ± 2 °C) during 2 days to make sure that complete dissolution was reached before use. This stock solution was stored in the darkness at 4 °C until use. Synthetic solution (SS) of atrazine was made by diluting the atrazine stock solution in deionized water and a stirring time around 20 min was fixed to ensure homogenization of the solution before each test. Final concentrations of synthetic solution atrazine were 10 and 100 µg L^{-1}. In order to increase the electrical conductivity in the solution, 30 mM of sodium sulfate salt (Na_2SO_4) was added. Likewise, the catalytic ferric ions was added using iron(II) sulfate heptahydrate ($FeSO_4.7H_2O$) supplied from Fisher Scientific (Toronto, ON, Canada). The initial pH was adjusted to 3.0 using sulfuric acid (0.1 M) supplied from Fisher Scientific (Quebec, QC, Canada). The names of the five major by-products of ATZ, their molecular formula and their retention time (liquid chromatography) are reported in SM1 (Table).

2.2. Surface water sampling and atrazine spiking

Surface water effluent (SWE) was sampled from agricultural areas beside intensive crops production (corn and soybean crops) where herbicides are often used. The sampling was carried out in the Nicolet River located in the province of Quebec (Canada). The SWE was collected, stored in polypropylene bottles and kept at 4 °C until use. The SWE had an initial content of soluble chemical oxygen demand (COD) of 92 ± 3.5 mg L^{-1}, pH of 6.7 ± 0.4, alkalinity of 1.4

meq L^{-1}, conductivity of 171.78 ± 18.32 µS cm^{-1}, turbidity of 9.05 ± 0.46 NTU, and atrazine (ATZ) concentration of 0.083 ± 0.016 µg L^{-1}. In view of testing the PEF process under different experimental conditions and to simulate a level of ATZ contamination most often encountered in surface water, SWE was enriched with 10 µg L^{-1} of ATZ.

2.3. Electrolytic reactor setup

In all tests, a total volume of 5 L of artificially contaminated water was used. The working volume of the electrolytic cell was 1.5 L, whereas 3.5 L was required for the recirculation tank. The treatment of ATZ was carried out in batch mode with undivided cylindrical cell made of quartz material with a dimension of 35 mm (width) x 250 mm (length) x 140 mm (height). The cell reactor is perforated at 50 mm from the top and bottom to ensure the recirculation of water through the cell and mixing solution in the cell in the continuous mode by means of a peristaltic pump operated at a constant speed of 250 mL min^{-1}. The anode electrode (110 mm height x 100 mm width x 1 mm thick) was either made of niobium coated with boron doped diamond (Nb/BDD) having an effective area for reaction of 90 cm^2. The graphite carbon plates as cathode (110 mm height x 100 mm width x 5 mm thick) have a surface area of 110 cm^2. The anode and cathode were placed in parallel, fixed vertically at 20 mm from the bottom of the cell and the inter-electrode gap was 10 mm (SM2). The anode and cathode were connected respectively to the positive and negative outlets of a DC power generator. The electrical current was applied to the electrodes using a digital DC generator model DCS40-75E (Sorensen DCS series, San Diego, USA) with a maximum current rating of 75 A, an open circuit potential of 40 V, and with a power of 3000 W. The PEF trials were made with different light irradiations, namely: fluorescent high intensity UV lamp model B-100 AP (100 W) which has a black filter. When the filter is attached, the wavelength and light intensity of the lamp are respectively 365 nm, and 125 mW cm^{-2}. When the filter is not fixed, the irradiation of the lamp is similar to AM 1.5 solar illumination conditions and the light intensity is 300 mW cm^{-2}. The light intensity of the fluorescent lamp was measured with a photometer radiometer data logger DO 9721 supplied by Delta Ohm (Padova, Italy). The other source of irradiation is the mercury vapor lamp model 3SC9 pen ray lamp (11 W, 254 nm, light intensity = 5.4 mW cm^{-2}). Her light intensity was measured with a photometer (Model PS-3, 99-0057-01, UVp Company, USA).

2.4. Experimental procedure

The first set of experiments was conducted to compare the removal efficiencies of ATZ using anodic oxidation with H_2O_2 (AO - H_2O_2), electro-Fenton process (EF) and photoelectro-Fenton process (PEF). AO - H_2O_2 process consist in treating ATZ using an electrochemical reactor comprising of Nb/BDD (anode) and graphite (cathode) on which H_2O_2 could be generated. EF process was carried out in the presence of 0.1 mM Fe^{2+} (corresponding to 27 mg L^{-1} of $FeSO_4.7H_2O$ used as catalyst for H_2O_2 decomposition) during AO - H_2O_2 process. PEF process combined EF process under UV irradiation. Experiments were carried out during 300 min of treatment time. A volume of 5 L of solutions containing 100 µg L^{-1} of ATZ at pH 3.0, in the presence of 30 mM of Na_2SO_4 was subjected to treatment at a current density of 2 mA cm^{-2}.

A second set of experiments consisted to test the influence of different operating parameters during the treatment of synthetic solution (SS) containing ATZ (100 µg L^{-1}). Operating parameters, such as light wavelength (254, 364 and 567 nm), current density (1.0 - 18.2 mA cm^{-2}) in the absence or in the presence of natural organic matter (humic acids, 5.0 and 10.0 mg L^{-1}) were investigated. The third set of experiments consisted to apply the best operating conditions of PEF process for the treatment of SWE enriched with 10 µg L^{-1} of ATZ. The fourth set of experiments consisted to increase the initial concentration of ATZ to 10 mg L^{-1} in order to identify by-products such as cyanuric acid (CA) during the treatment of SWE using PEF process.

All experiments were carried out in batch mode and the reactor was rinsed several times with distilled water before each experiment. Likewise, the experiments were repeated in triplicate to verify the reproducibility. During all assays at room temperature, the reactor was protected from any external light with a dark cover. Then, 20 mL of the treated solution was taken out at different time intervals between 0 and 420 min, and then analyzed with LC-MS/MS. Likewise, at different time intervals, the pH and temperature inside the electrolytic cell were measured using a pH-meter (Accumet Excel XL25-pH/mV/Temp/Ion Meter, Fisher Scientific Co).

2.5. Analytical methods

2.5.1. Measurement of residual hydrogen peroxide concentration

The capacity of EPC reactor to generate H_2O_2 was tested under UV irradiation lamp using distilled water containing Na_2SO_4 (0.05 M) which insured a high level of the electrical conductivity. During the trials, the residual H_2O_2 concentration was measured using volumetric dosage (Sigler and Masters 1957). The cerium ion solution (Ce $(SO_4)_2$, $2(NH_4)_2$ SO_4, 2 H_2O), (5.88 x 10^{-3} M) was used under acidic conditions (H_2SO_4, 9 N) in the presence of three drops of ferrous ortho-phenanthroline ($\mathrm{Fe(o-phen)_3^{2+}}$) used as an indicator. The gradual change of the solution color from red to the blue indicates a total oxidation of hydrogen peroxide. The residual concentrations of H_2O_2 were determined with H_2O_2 calibration curve by plotting the cerium volume (mL) as a function of H_2O_2 concentration (from 0 to 3.94 x 10^{-3} M).

2.5.2. Extraction of herbicide compounds in surface water

Atrazine and its by-products compounds were extracted from water by solid phase extraction (Sep-Pak cartridge octadecyl C18, Waters, Ontario, Canada) with a solvent mixture of $MeOH/H_2O$. Cartridges were conditioned by passing 5 mL of MeOH and 5 mL of milli-Q water by gravity. A volume of 200 mL of river water was treated by passing through the cartridges using a Visiprep^{tm} SPE vacuum manifold. Then, the cartridges were washed with 5 mL of methanol solution (5%) in milli-Q water, and the compounds were eluted with 5 mL of methanol. Elution was performed by gravity in conical tubes provided for this purpose and the solution was evaporated with a gentle stream of nitrogen. After evaporation the final volume of 1 mL was injected into the liquid chromatography mass spectrometer (LC-MS/MS, TS Quantum Access, Thermo Scientific, Mississauga, Ontario, Canada).

2.5.3. Measurement of ATZ and by-products concentrations

During the experiments, residual concentrations of ATZ and its by-products were quantified by liquid chromatography mass spectrometer (LC-MS/MS, Thermo TS Quantum Access). The chromatographic column used was the Hypersil Gold aQ C8 (Thermo Hypersil Ltd., Runcorn, UK) with a particle size of 3.0 μm and a 100 mm length x 2.1mm inner diameter. The analytes were separated using an ammonium acetate-buffered binary mobile phase and subsequently detected by positive electrospray ionization tandem mass spectrometry. The concentration of each identified component is determined using the internal standard technique. The mobile phase composition was acetonitrile and 5mM ammonium acetate at pH 6.5, using the solvent gradient 15:85 (0 min), 80:20 (8 min), and 15:85 (20 min) and the flow rate was 0.25 mL min^{-1}. Calibration standard solutions between 1.0 μg L^{-1} and 100 μg L^{-1} of ATZ and four of its degradation products (ATZ-OH, DEA, DIA and DEDIA) were prepared in water by serial dilution of the stock solutions. The stock solutions were preserved in methanol and stored at 4 °C until use. Quality control included chromatographic and extraction blanks, duplicates (every 10 samples) and fortified samples (every 15 injections) and control samples made from commercial standards. The instrumental detection limits for ATZ and DEA were 0.2 μg L^{-1}: DIA and DEDIA were 1 μg L^{-1} and ATZ-OH was 0.4 μg L^{-1}. The linear regression equation of the calibration curve ($Y = 0.0627x - 0.00042$, $R^2 = 0.9999$) allow to determine the remaining ATZ concentration and define the efficiency of the different processes studied such as PEF process. Nitrogen was used as a sheath and auxiliary gas. Working conditions were as followed: spray voltage was 3500 V and capillary temperature was 350 °C.

2.5.4. Measurement of cyanuric acid concentration

During the step of mineralization of ATZ, the cyanuric acid concentration was evaluated and quantified by liquid chromatography mass spectrometer (LC-MS/MS, Thermo TSQ Quantum Access). The chromatographic column used was the Hypersil Gold C18 (100 mm lengh x 2.1mm inner diameter) heated at 30 °C. The analytes were separated using an acetic acid buffered binary mobile phase and subsequently detected by negative electrospray ionization tandem mass spectrometry. The mobile phase composition was acetic acid solution (0.1%) in milli-Q water and methanol, using the solvent gradient 90:10 (0 min), 20:80 (5 min) and 90:10 (9 min) : the flow rate was 0.20 mL min^{-1}. Nitrogen was used as a sheath and auxiliary gas. Working conditions were as followed: spray voltage was 4000 V and capillary temperature was 350 °C. Calibration standard solutions between 12.5 µg L^{-1} and 245 µg L^{-1} of cyanuric acid were prepared in milli-Q water and the instrumental detection limit of cyanuric acid was 3.0 µg L^{-1}.

2.5.5. Measurement of inorganic ions, total organic carbon and chemical oxygen demand

The anion Cl^{-} released into the treated solutions during electrolysis was determined by ion chromatography using Dionex ICS-2000 Basic Ion Chromatography System (Sunnyvale, CA, USA) fitted with an IonPac column AS18, 4 x 250 mm and AG18, 4 x 50 mm. The sensitivity of this detector was improved from electro-chemical suppression using an AERS 500, 4 mm self-regenerating suppressor. Measurements were made with a solution of 23 mM KOH for anion-exchange column. Ammonia concentration was determined according to the analytical method proposed by LACHAT Instrument (QuikChem® Method 10-107-06-2-B). TOC was measured using a Shimadzu TOC 5000A analyzer (Shimadzu Scientific Instruments, Kyoto, Japan). The chemical oxygen demand (COD) was measured by colorimetric method in presence of potassium dichromate according to the method (MA. 315-DCO 1.0) proposed by CEAEQ (CEAEQ 2003).

2.6. Estimation of energy consumption

During the electrolysis, the energetic efficiency of EAOPs processes such as the energy consumption per unit volume (Eq. (8)) and the mineralization current efficiency (Eq. (9)) were calculated from different equations.

$$\text{EC (kWh m}^{-3}) = \frac{E_{cell}\, I\, t}{V_s} \qquad (8)$$

where E_{cell} is the voltage of generator (V), I is the applied current (A), t is the time of electrolysis and Vs is the solution volume (L).

In the case of the mineralization current efficiency (Eq. (9)), the equation was

$$\text{MCE (\%)} = \frac{nFV_s(\Delta\text{TOC})}{4.32\ \text{X}10^7 mIt} \qquad (9)$$

where F is the Faraday constant (96487 C mol^{-1}), Vs is the solution volume (L), Δ(TOC) is the decay of TOC (mg L^{-1}) in solution, m is the number of carbon atoms of ATZ, I is the applied current (A), n is the number of electrons consumed per ATZ molecule, and t is the time to treat the solution. According to Borràs et al. (2010), the number of carbon atoms of ATZ and the number of electrons consumed during the mineralization was shown in this reaction (Eq. (10)) :

$$\text{C}_8\text{H}_{14}\text{ClN}_5 + 31\text{H}_2\text{O} \rightarrow 8\text{CO}_2 + \text{Cl}^- + 5\text{NO}_3^- + 76\text{H}^+ + 70\text{e}^- \qquad (10)$$

The energy consumption per unit of TOC mass (Eq. (11)) was calculated by the equation :

$$\text{EC}_{\text{TOC}}(\text{kWh mg}^{-1}\ \text{TOC}) = \frac{E_{cell}\, I\, t}{(\Delta\text{TOC})V_s} \qquad (11)$$

where E_{cell} is the voltage of generator (V), I is the applied current (A), t is the time of electrolysis, Δ(TOC) is the decay of TOC (mg L^{-1}) in solution and Vs is the solution volume (L).

3. RESULTS AND DISCUSSION

3.1. Linear voltammetry

The aim of these experiments was to select the anode having a higher O_2 overpotential value. The linear voltammetry of three different anodes (Nb/BDD, Ti/PbO_2, and Ti/Pt) was study in the presence of 7.04 µM of Na_2SO_4 at 500 rpm, with a scan rate of 2 mV s^{-1} at room temperature (around 22 °C). Based on the Comninellis model, two types of electrodes can be distinguished: active electrodes (such as Ti/Pt) and non-active electrodes (such as Nb/BDD) (Comninellis 1994, Brillas et al. 2009). The oxidation of H_2O into O_2 appeared at 0.7 V on Ti/Pt and at 1.2 V on Ti/PbO_2, whereas it appeared at 1.5 V on Nb/BDD (SM3). This test shows that Nb/BDD had the highest overpotential value. Likewise, it was found that only Nb/BDD can oxidize the sulfate ions into peroxodisulfate anions (Eq. (12)).

$$2\,SO_4^{2-} \rightarrow S_2O_8^{2-} + 2e^- \qquad (12)$$

Consequently, Nb/BDD was selected as the most effective working anode for the degradation of ATZ and its main by-products in water.

3.2. Hydrogen peroxide production

The hydrogen peroxide can be electrochemically generated at the electrode cathode by oxygen reduction (Brillas et al. 2009, Sirés et al. 2014, Komtchou et al. 2015). This reduction of dissolved oxygen was more favourable in acidic condition for which H_2O_2 is more stable (Komtchou et al. 2015). The aim of these experiments was to evaluate the capacity of the electrolytic cell (comprised of graphite cathode and BDD anode) to produce H_2O_2 in the presence of Na_2SO_4 (0.03 M) in the solution (5 L), but in the absence of ATZ. Fig. 1 shows H_2O_2 concentrations generated during electrolysis for different current densities imposed. The maximum H_2O_2 concentration (4.15 mg H_2O_2 L^{-1}) was obtained with 18.2 mA cm^{-2} (curve c), whereas a minimum H_2O_2 concentration (1.23 mg H_2O_2 L^{-1}) was recorded with a current density of 2.0 mA cm^{-2} (curve a). As it can be seen in Fig.1, H_2O_2 increased with current intensity. These results were consistent to those recorded by Brillas et al. (2000) and Komtchou et al. (2015) while using advanced electrochemical oxidation processes (such as electro-Fenton and photoelectro-Fenton processes) for carbamazepine and dichlorophenoxyacetic acid removal from waters. These result confirmed that graphite can be used as a cathode material to produce H_2O_2. Likewise, in the electrolytic cell H_2O_2 can be decomposed into hydroxyl radical (Eq. (13)) in the presence UV light (Sirés et al. 2014):

$$\mathrm{H_2O_2} + \ h\nu \ \rightarrow \ 2\,\mathrm{OH}^{\bullet} \qquad (13)$$

The comparison between the curves (c) and (d) in Fig. 1, gives the estimation of residual H_2O_2 concentrations in the electrolytic cell after 60 min of electrolysis under UV light (λ = 254 nm) when applying a current density of 18.2 mA cm^{-2}. H_2O_2 concentration varying from 2.14 to 4.15 mg H_2O_2 L^{-1} was measured in the absence of UV irradiations (curve c) when a current density of 18.2 mA cm^{-2} was applied. By comparison, residual concentrations ranging from 1.4 to 3.5 mg H_2O_2 L^{-1} were recorded in the presence of UV irradiations (λ = 254 nm) (curve d) for the same current density of 18.2 mA cm^{-2}. The relatively low H_2O_2 concentration that was recorded in the presence of UV irradiation can be attributed to hydroxyl radical formation (the decomposition of H_2O_2 into $^{\bullet}OH$).

3.3. Comparison between electrochemical advanced oxidation processes in treating water contaminated by ATZ

The first set of experiments was carried out to compare the degradation efficiencies of ATZ and its by-products using AO- H_2O_2, EF and PEF processes. Fig. 2a shows ATZ concentration changes using different advanced oxidation processes operated at a current density of 2 mA cm^{-2}. After 90 min of treatment, the degradations of ATZ were 45.42%, 60.89% and 99.11% using AO - H_2O_2, EF and PEF processes, respectively.

3.3.1. AO - H_2O_2 process

ATZ removal using AO - H_2O_2 process results from hydroxyl radicals generated on the surface of BDD by anodic oxidation of water (Eq. (14)).

$$\mathrm{BDD} + \mathrm{H_2O} \rightarrow \mathrm{BDD(HO^{\bullet})} + \mathrm{H^+} + \mathrm{e^-} \quad (14)$$

The degradation of ATZ can also be attributed to indirect oxidation obtained with H_2O_2 and $S_2O_8^{2-}$ simultaneously generated at the cathode and anode, respectively. The rate constant of ATZ degradation using AO - H_2O_2 process was about 0.007 min^{-1}. The concentration of major by-products is very high (Fig. 2b) such as DEA (29 µg L^{-1}) and DEDIA (12 µg L^{-1}) after 30 min of treatment. The quantity of oxidants such as $HO^{\bullet}$ radical in the electrochemical cell was possibly insufficient to attack simultaneously high amounts of both ATZ molecule and its major by-products.

3.3.2. EF process

In the EF process, ATZ removal efficiency was 60.89% after 90 min of treatment (Fig. 2a) and the corresponding degradation rate constant was about 0.01 min^{-1}. The degradation of ATZ is due to the presence of ferrous ions used as catalyst for the H_2O_2 decomposition into $HO^{\bullet}$ (Eq. (4)). Also, the heterogeneous reaction of adsorbed hydroxyl radical generated by BDD anode (Eq. (14)) and the complementary reactions of oxidants generated in solution (such as H_2O_2, $HO_2^{\bullet}$, and $S_2O_8^{2-}$) increase the degradation rate of ATZ. During the electrolysis, the majors by-products decrease in this order DEA > DIA > DEDIA > ATZ-OH (Fig. 2c). After 240 min of treatment, only the concentration of DEDIA (4.7 µg L^{-1}) was higher than the detection limit. As it can be seen, the EF process was more effective than AO - H_2O_2 process probably owing to the more appropriate oxidizing conditions obtained in the case of EF process (more reactive oxygen species generated).

3.3.3. PEF process

In the PEF process using UV light (254 nm) in the presence of H_2O_2 and ferrous ions, the degradation efficiency recorded was more than 99% after 90 min of treatment time (Fig. 2a) and the rate constant of degradation was about 0.05 min^{-1}. This fast disappearance of ATZ can be attributed to three mains electrochemical/chemical reactions that took place simultaneously for hydroxyl radical formation: i) Fe^{2+} regeneration from photoreduction of $Fe(OH)^{2+}$ that leads to $HO^{\bullet}$ formation (Eq. (6)); ii) decomposition of H_2O_2 into hydroxyl radical in the presence of UV_{254} light (Eq. (13)) which generates the hydroxyl radical in solution; iii) photolysis of peroxodisulfate anions (Eq. (15)) gives a sulphate anion radical which is a very strong oxidant reagent (Herrmann 2007, Criquet and Leitner 2009):

$$S_2O_8^{2-} + hv_{(248\text{ to }351\text{ nm})} \rightarrow 2SO_4^{-\bullet} \qquad (E^0 = 2.43\text{ V/NHE}) \qquad (15)$$

and (d) dechlorination of ATZ molecules which take place by heterolytic cleavage of ATZ in polar solvents such as water (Chen et al. 2009) (Eqs. (16) to (18)).

$$ACl + hv \rightarrow ACl^* \qquad (16)$$

$$ACl^* \rightarrow A^+ + Cl^- \qquad (17)$$

$$A^+ + H_2O \rightarrow AOH + H^+ \qquad (18)$$

During the PEF process, the concentrations of the major by-products decrease in the following order: ATZ-OH > DEA > DIA > DEDIA (Fig. 2d). The concentrations of major by-products are very low as compare to AO- H_2O_2 and EF processes. The high concentration of ATZ-OH (around 8.5 µg L^{-1} at 30 min) can be explained by mechanism of dechlorination of ATZ under irradiation UV light (254 nm). After 180 min of treatment, the residual concentrations of ATZ-OH, DEA and DIA were below the detection limits. The concentration of DEDIA (3.1 µg L^{-1}) was relatively low compared to those recorded for AO - H_2O_2 and EF processes. According to Komtchou et al. (2016b), DEDIA was formed by dealkylation of both DEA and DIA. This behaviour can explain the persistence of this by-product and the low reactivity with oxidants such as hydroxyls radicals using AO - H_2O_2, EF and PEF processes. The degradation rate of ATZ (including its by-products) increased while using PEF process followed by EF and AO - H_2O_2 processes. The energy consumptions (Eq. (8)) were respectively estimated to 76.0, 60.8 and 30.4 Kwh m^{-3} for AO - H_2O_2, EF, and PEF processes. To effectively remove ATZ and its by-products from water, the PEF process was selected for the next step of the experiments.

3.4. Optimization of PEF process for the treatment of water contaminated by ATZ

3.4.1. The wavelength effect

In the PEF process, the light intensity and wavelength are the important parameters which affect the effectiveness of the treatment. In order to understand the impact of the light source, the experiments were carried out using different wavelengths: UVC (λ = 254 nm), UVA (λ = 365 nm) and visible light (λ_{max} = 576 nm). After 90 min of treatment, the removal efficiencies of 69.3%, 80.4% and 99.1% were obtained using 365 nm, visible light and 254 nm, respectively (Fig. 3a). The use of UVC irradiation gave the best results because the UVC irradiations induce the photolysis of different species present in the system such as $Fe(OH)^{2+}$, $S_2O_8^{2-}$ and ATZ (Criquet and Leitner 2009, Borràs et al. 2010, Komtchou et al. 2016b). Likewise, the generation of $HO^{\bullet}$

from the homolytic cleavage of H_2O_2 improves the degradation of ATZ and its by-products (Fig. 3b). By comparison, under UVA irradiation the decomposition of H_2O_2 into $HO^•$ is not possible because H_2O_2 does not absorb at all above 320 nm (Sum et al. 2005). Thereby, the action of UVA light increases the conversion of Fe^{3+} to Fe^{2+} (Eq. (5)). During the electrolysis using UVA, the maximum concentration of by-products (Fig. 3c) was 10.12 µg L^{-1} (DIA) and 9.18 µg L^{-1} (DEA). The low concentration of ATZ-OH (1.45 µg L^{-1}) indicated that the dechlorination of ATZ molecules was reduced because the wavelength is higher than 254 nm. After 180 min of treatment, only the concentration of ATZ-OH was below the detection limit.

In the case of ATZ degradation under visible light, a high intensity of irradiation which enter into the solution increase the photoreduction of dissolved ferric iron to ferrous iron. Also, the photodecarboxylation of complexes between Fe(III) and the intermediates by-products is improved by the additional absorption at $\lambda > 400$ nm. Likewise, during the PEF process under visible light the temperature increased from 18.9 to 39.3 °C after 300 min of treatment. According to Lee and Yoon (2004), the visible light is a heat source which increase the activity of the photo Fenton systems. This was the reason for which the degradation of ATZ and its by-products was higher under visible light than that recorded under UVA light using PEF process (Fig. 3d). During the electrolysis, the concentrations of the major by-products decrease in the following order: DIA > DEA > DEDIA > ATZ-OH. The by-product DEDIA was detected and quantified in treated solution after 300 min of treatment regardless of the wavelength imposed.

The energy consumption (Eq. (8)) was estimated to 59.2, 53.2 and 30.4 Kwh m^{-3} using PEF (365 nm), PEF (visible light) and PEF (254 nm), respectively. Thus, the wavelength of 254 nm was selected for the next step of the study.

3.4.2. The current density effect

In the electrochemical advanced oxidation processes (such as PEF process), the values of current density affect the effectiveness of the treatment because it regulates the generation of hydroxyl radicals. Thus, different current densities ranging between 1.0 to 18.2 mA cm^{-2} were tested during the degradation of ATZ (100 µg L^{-1}) for an initial pH 3.0 with 0.1 mM Fe^{2+}. Table 1 shows a faster and higher ATZ degradation while increasing the current density. After 15 min of treatment, the percentages of ATZ removal were 99.57%, 68.18%, 56.85% and 38.12% respectively with 18.2, 9.1, 4.5 and 1.0 mA cm^{-2} (corresponding to 2000, 1000, 500 and 100 mA). The increase of the effectiveness of PEF process while increasing the current density can be attributed to three main points: (i) high production of hydroxyl radicals on BDD anode material for high current densities confirming the efficacy of BDD anode in the PEF process; (ii) the rate of H_2O_2 production increases with current densities (Fig. 1) so that the Fenton's reaction (Eq. (4)) can be accelerated, and (iii) the increase in H_2O_2 concentration in solution contributes to generate more hydroxyl radicals owing to the decomposition of H_2O_2 in the presence of UV irradiation (Eq. (13)). The reaction of ATZ with hydroxyl radicals can be described by an apparent first-order kinetic model (Eq. (19)).

$$\mathrm{v} = \frac{\mathrm{d\,[ATZ]}}{\mathrm{dt}} = k_{\mathrm{abs,\ ATZ}}\,[\mathrm{HO^{\bullet}}][\mathrm{ATZ}] = k_{\mathrm{app}}[\mathrm{ATZ}] \qquad (19)$$

The apparent rate constants, k_{app}, were calculated in Table 1 according to the linear regression from the slope of a plot of ln (C_0/C), where C_0 is the initial concentration and C is the concentration of ATZ at time t (Eq. (20)).

$$\ln\frac{\mathrm{C_0}}{\mathrm{C}} = k_{\mathrm{app}} * \mathrm{t} \qquad (20)$$

The different values of kinetic rate constants (k_{app}) came from correlation coefficients R^2 higher than 0.96. Table 1 gives the values of k_{app} and half-life of ATZ using PEF process. Comparing the half-lives of ATZ, it can be seen that the degradation is faster using 18.2 mA cm^{-2}.

During the PEF process, the concentration of ATZ-OH decreases when the current densities increase (Fig. 4). The maximum concentration of ATZ-OH was 12.16, 8.20, 6.15 and 4.65 µg L^{-1} respectively with 1, 2, 4.5 and 9.1 mA cm^{-2} (Fig. 4a to Fig. 4c, and Fig. 3b). This behaviour proves that the attack of ATZ molecules is mainly due to the action of $HO^{\bullet}$ radicals. Likewise, treatment time required to remove the by-products in the solution decreases with an increase of the current densities because the production of oxidants such as $HO^{\bullet}$ radical was relatively high for high current densities. Thereby, during the electrolysis at 18.2 mA cm^{-2}, all the concentrations of major by-products were less than their limit of detection after 45 min of treatment. The persistent by-product DEDIA was totally removed from the treated solution. In order to reduce the electrolysis time, a current density of 18.2 mA cm^{-2} was selected for the next step of this study.

3.4.3. The humic acids effect

The humic acids (HA) are one of the major constituents of the natural dissolved organic matter in the aquatic environment. Several author's showed that the photolysis of ATZ in the presence of HA decreases because HA react with hydroxyl radicals (Torrents et al. 1997, Prosen and Zupančič-Kralj 2005). But according to Aguer et al. (1999), the photochemical excitation of HA under irradiation at 254 nm generate hydrated electrons which can produce a strong oxidant in the presence of oxygen. The aim of these tests was to assess if the presence of HA in aqueous solution may increase or decrease the degradation of ATZ using PEF process. Fig. 5a shows ATZ degradation (100 µg L^{-1}) without HA and with 5.0 and 10.0 mg L^{-1} of HA at an initial pH 3.0. After 10 min of treatment, the percentages of ATZ removal were 80.8%, 90.5% and 97.4% while using 10.0, 5.0 and 0.0 mg L^{-1} of HA, respectively. According to Fukushima and Tatsumi (2001) and Ou et al. (2007), the HA have abilities to complex Fe(III) and this complex increase with HA concentration. Therefore, the photochemical excitation of HA can generated H_2O_2 in the presence of oxygen (Eqs. (21) to (23)). Likewise, the photoreduction of the complex Fe(III)-HA regenerated Fe^{2+} and the degradation of HA occurs (Eq. (24)).

$$\mathrm{HA} + \mathrm{hv} \rightarrow \mathrm{HA}^* \qquad (21)$$

$$\mathrm{HA}^* + \mathrm{O_2} \rightarrow \mathrm{HO_2^\bullet} \qquad (22)$$

$$2\,\mathrm{HO_2^\bullet} \rightarrow \mathrm{H_2O_2} \qquad (23)$$

$$\mathrm{Fe(III)} - \mathrm{HA} + \mathrm{hv} \rightarrow \mathrm{HA^{\bullet +}} + \mathrm{Fe^{2+}} \qquad (24)$$

On the other hand, the complex $Fe(OH)^{2+}$ decreases when the complexes Fe(III)-HA increases in the presence of HA. Therefore, the photoreduction of $Fe(OH)^{2+}$ which generated hydroxyl radical decreases in the reactor. Secondly, it is possible that the presence of HA reduces the absorption light and the photodecomposition of H_2O_2 into hydroxyl radicals. Consequently, the parasitic reaction occurring between H_2O_2 and $HO^\bullet$ increases in the reactor (Eq. (25)).

$$\mathrm{H_2O_2} + \mathrm{HO^\bullet} \rightarrow \mathrm{H_2O} + \mathrm{H_2O^\bullet} \qquad (25)$$

Thirdly, the regeneration of Fe^{2+} come from electroregenerated Fe^{2+} at the cathode (EF process), photoreduction of $Fe(OH)^{2+}$ and Fe(III)-HA complexes. Thereby, the parasitic reaction occurring between Fe^{2+} and $HO^\bullet$ increase with high regeneration of Fe^{2+} in the reactor.

The fact that HA can react with hydroxyl radicals explain why the degradation of ATZ decreased when the concentration of HA increased in water. In the case of by-products such as ATZ-OH, some complexes compounds can be formed with HA (Martin-Neto et al. 2001). This behaviour can explain why the degradation of ATZ-OH was not rapidly recorded in the presence of HA

(Fig. 5c and 5d compare to Fig. 5b). Likewise, in the absence of HA, all the concentrations of major by-products such as DEDIA were less than the limit of detection (Fig. 5b). But in the presence of HA, the persistent by-product DEDIA was detected in the treated solution. This observation suggests that the HA can compete with ATZ and its by-products during water treatment.

It is worth noting that, in the presence of natural organic matter (such as humic substances), these substances can act as micellar aggregates with hydrophilic exteriors surfaces and predominantly hydrophobic interiors (Guetzloff and Rice 1994, Chien et al. 1997, von Wandruszka 1998, de Melo et al. 2016). Thus, atrazine can bind to humic substance via cooperative hydrogen bonds and hydrophobic interactions that are stable only in the hydrophobic environment found at the interiors of humic micelles (Chien et al. 1997). In view of better understanding of atrazine degradation, a study of the micellization and micellar solubilization of atrazine in the presence of humic acids should be carried out by using electron paramagnetic resonance (EPR) spectroscopy.

3.5. Application of PEF process for the treatment real agricultural surface water

The effectiveness of PEF process to treat surface water (initial ATZ concentration < 0.1 µg L^{-1}) spiked with ATZ was evaluated at a current density of 18.2 mA cm^{-2}. During these tests, we did not add HA because this river water already contained natural dissolved organic matter. Before the treatment, the surface water was spiked with ATZ (10 µg L^{-1}). This concentration was the maximum concentration found in Quebec rivers (Giroux and Pelletier 2012) after ATZ applications on the crops. The sampling of water was performed on August 10, whereas the ATZ application in this agricultural area was carried out around the end of June. Then, it was expected that the sampled water should contained low residual concentration of ATZ.

After settling by gravity (without filtration), the supernatant was analyzed by ICP-AES Varian Vista AX to determine the metals concentration (*e.g.* Fe total, P total). The solid phase extraction allowed to extract the target compounds from water and chromatographic analysis showed the presence of ATZ (0.083 ± 0.016 µg L^{-1}), DEA (0.024 ± 0.006 µg L^{-1}) and ATZ-OH (0.013 ± 0.004 µg L^{-1}). The DIA and DEDIA were not detected. Table 2 gives the result of the chemical analysis of the river water. The following metals were found in low concentrations (almost below 25 µg L^{-1}) : Ni, Sr, Cu, Mn, B, Ba, Cr, Ti, V and Zn. The presence of iron (Fe total) in water samples was an advantageous for PEF process application without adding any chemical. But the presence of natural scavenging agents of $HO^{\bullet}$ radicals in water such as carbonate ions may reduce the effectiveness of PEF process to remove ATZ from surface water.

Different tests were carried out using real surface water contaminated by ATZ: 1) treatment without adding Fe ([Fe naturally present in water] ≈ 0.01 mM); 2) Treatment with addition of Fe_{total} ([Fe] = 0.1 mM) using the iron (II) in form of sulphate heptahydrate. The tests were respectively performed without pH adjustment (around pH = 6.7) and with pH adjustment (around pH = 3.1). Fig. 6 shows that in spite of the presence of radical scavenger (*e.g.* carbonate ions) and the complexation of Fe(III) by Cl^- or SO_4^{2-}, the PEF process was more effective to remove ATZ from surface water when the pH value was adjusted near to 3.0. Indeed, after 25 min of treatment, the ATZ removal was 96.0% with 0.01 mM of iron (k_{app} = 0.13 min^{-1}) and 100% with 0.1 mM of iron (k_{app} = 0.17 min^{-1}).

Nonetheless, the percentage of ATZ removal was different while increasing the concentration of iron at pH 3.1 (Fig. 6a). This observation indicates that is not necessary to use high concentrations of iron to remove ATZ from water by PEF process. On the other hand without a pH adjustment (pH = 6.7), ATZ removal was 44.75%, whereas it was 32.96% with 0.1 mM of iron after 30 min of treatment. According to De Laat and Gallard (1999) and Brillas et al. (2009), the ferric ions precipitate in solution ($Fe(OH)_3$) at pH > 5.0. Thereby, hydroxyl radicals formation decreased because of photoreduction of $Fe(OH)^{2+}$. Therefore, the degradation of ATZ was mainly due to anodic oxidation using BDD and the photolysis of oxidant such as H_2O_2.

Notwithstanding the treatment during the first 10 min, the Fig. 6b shows that the removal of ATZ with 0.1 mM of iron is higher than without iron adjustment. This efficiency of PEF process with 0.1 mM iron at 10 min of treatment time can be justified by Fenton's reaction. After oxidation of Fe(II), the high concentration of ferric ions can be combined with the hydroxide ions leading to the formation of iron hydroxides $Fe(OH)_3$. This behaviour causes the decay of the degradation curve and the parasitic reactions linked to the presence of iron hydroxides explained why after 15 min of treatment, the position of the curve with 0.1 mM of iron is below the curve without iron adjustment.

During the electrolysis at pH 3, the analyses with chromatography identified DEDIA, DEA and ATZ-OH as being the by-products. At pH 6.7, DEA and ATZ-OH were the only ones of the by-products that were detected. At pH 3.1 with 0.1 mM of iron, the Fig. 6c shows that the maximum concentration of by-products was obtained, but the treatment time was short and the removal of by-products has been not optimal. However, at pH 6.7 with 0.1 mM of iron, the by-products (DEA and ATZ-OH) increased gradually (Fig. 6d). The absence of others by-products such as DEDIA and DIA suggests that the degradation of ATZ was limited at this value of pH (pH=6.7). Therefore, this result confirms the efficiency of PEF process at pH value around 3 because the generation of oxidants (such as $HO^{\bullet}$ radicals) was relatively high.

3.5.1. Mechanisms of the oxidation of ATZ and its by-products

To maximize the detection of by-products such as cyanuric acid, the initial ATZ concentration imposed was relatively high (around 10 mg L^{-1} or 0.046 mM). The removal of ATZ was fast and after 180 min of treatment, the concentration was below the detection limit (Fig. 7a). The chromatograms at 0, 120, 300 and 420 min of treatment show the variations of the main by-products such as cyanuric acid (SM4). During the electrolysis, the concentrations of by-products decreased in the following order: DEDIA > DIA > DEA > ATZ-OH > CA. The maximum concentration values of these four primary by-products were 1200 µg L^{-1} (DEDIA), 145 µg L^{-1} (DIA), 128 µg L^{-1} (DEA) and 105 µg L^{-1} (ATZ-OH) after 60 min of treatment (Fig. 7b). In the case of cyanuric acid, the concentration increased gradually and the maximum concentration was 23 µg L^{-1} after 420 min of treatment (Fig. 7c). This behaviour can be explained because CA is one of the most persistent by-products from ATZ degradation and having low reactivity with hydroxyls radicals (Borràs et al. 2010, Oturan et al. 2012). In the other hand, the CA can be removed with a high current density such as 50 and 40 mA cm^{-2} (Borràs et al. 2010, Oturan et al. 2012). This argument justified why in this study after 420 min of treatment, the concentration of CA did not decrease in our electrochemical cell, despite that a current density imposed of 18.2 mA cm^{-2}.

The specific mass and ionic spectra of degradation products gave the secondary by-products of ATZ, which was formed by dechlorination, dealkylation and alkylic-oxidation mechanisms. However, more by-products were not clearly identified (name and molecular formula) because some values of m/z gave unidentified intermediates compounds (SM 5). Therefore, the possible pathways of ATZ degradation by hydroxyl radicals appears to be similar to those proposed by Komtchou et al. (2016b) using electrophotocatalytic process.

3.5.2. Mineralization and inorganic ions generated by ATZ degradation

The initial TOC concentration recorded in real surface water (river water) was 9.6 ± 0.16 mg L^{-1}. The residual TOC concentration recorded at the end of the treatment was 1.8 ± 0.06 mg L^{-1} (Fig. 8a). The reduction of TOC was 81.3% after 420 min treatment. This result indicates that a high fraction of ATZ and other fractions of some refractory organic matter were completely oxidized into water, giving carbon dioxide and inorganic ions. The consumed specific charge (Q, in Ah L^{-1}) during the electrolysis was very low (2.8 Ah L^{-1} after 420 min of treatment) compared to that recorded (18 Ah L^{-1}) by Borràs et al. (2010). In these conditions (2.8 Ah L^{-1} at 420 min), high mineralization of organic matter was recorded. To confirm this mineralization, NH_4^+ was detected (Fig. 8c) and the maximum concentration was 0.362 ± 0.045 mg L^{-1} (0.02 mM). During the electrolysis, the mineralization current efficiency (MCE) (Eq. (9)) was evaluated (Fig. 8b) and the maximum efficiency was 8.3%. This value explained why the degradation of ATZ was fast in the electrochemical cell. But this degradation produced the intermediates products such as cyanuric acid having low reactivity with hydroxyl radicals. Likewise, the energy consumption per unit of TOC mass (Eq. (11)) increases (Fig. 8d) and this proved that it is feasible to reduce the current density during the treatment. In the other hand, the COD measurements showed that in the treated solution (samples), the oxygen demand was below the limit of detection (3 mg L^{-1} O_2).

4. CONCLUSION

In this study, the presence of ATZ (≈ 0.1 µg L^{-1}) and its by-products was detected in the samples of Nicolet River in Quebec – Canada. The efficiency of the PEF process in acidic medium, using BDD anode to remove ATZ (10 µg L^{-1}) and its by-products in this river water samples was demonstrated. To the best of our knowledge, no other studies using the PEF process attempted to treat natural surface water, sampled in agricultural area and containing low concentration of ATZ. This was done in part considering the natural pH of water as well as in the presence of natural dissolved organic matter (humic acids). In the PEF process, the synergistic action of direct oxidation, indirect oxidation and photolysis (mediators and complexes) under UV irradiation increased the generation of $HO^{\bullet}$ radicals and other strong oxidants that removed atrazine from water. The degradation of atrazine led to cyanuric acid having low reactivity with hydroxyls radicals. Thereby, the cyanuric acid did not decrease in our electrochemical cell. Despite the presence of radical scavenger in surface water, the abatement of TOC was 81.25% after 420 min of treatment. Likewise, the high mineralization current efficiency and the low chemical reagents consumption proved that the PEF process was an environmentally friendly process. Nevertheless, the cost of energy consumption and UV lamps are the main drawback of this process. Therefore, the solar energy is the one of the alternative solution to reduce the energy consumption. The efficiency of the PEF process using solar light was also discussed in this study. But the PEF using UV light source reduces the time of treatment compared to solar light. Beyond all this, the optimum pH of the PEF process represents the principle obstacle to combine this process with biological treatment in a water treatment plant to remove refractory organic compounds such as pesticides. The next step should be the study of the micellization and micellar solubilization of atrazine in the presence of humic acids by using electron paramagnetic resonance (EPR) spectroscopy. This will help us to deeply understand the mechanism behind atrazine degradation using electrochemical advanced oxidation processes in the presence of natural organic matter.

Acknowledgments

We acknowledge the National Sciences and Engineering Research Council of Canada for their financial contribution to this study.

REFERENCES

Aguer, J., Richard, C. and Andreux, F. (1999) Effect of light on humic substances: production of reactive species. Analusis 27(5), 387-389.

Aquino, J.M., Miwa, D.W., Rodrigo, M.A. and Motheo, A.J. (2017) Treatment of actual effluents produced in the manufacturing of atrazine by a photo-electrolytic process. Chemosphere 172, 185-192.

Borràs, N., Oliver, R., Arias, C. and Brillas, E. (2010) Degradation of Atrazine by Electrochemical Advanced Oxidation Processes Using a Boron-Doped Diamond Anode. The Journal of Physical Chemistry A 114(24), 6613-6621.

Brillas, E., Calpe, J.C. and Casado, J. (2000) Mineralization of 2,4-D by advanced electrochemical oxidation processes. Water Research 34(8), 2253-2262.

Brillas, E., Sirés, I. and Oturan, M.A. (2009) Electro-Fenton Process and Related Electrochemical Technologies Based on Fenton's Reaction Chemistry. Chemical Reviews 109(12), 6570-6631.

CEAEQ (2003) Détermination de la demande chimique en oxygène dans les effluents: méthode de reflux en système fermé suivi d'un dosage par colorimétrie avec le bichromate de potassium, p. 14, Centre d'Expertise en Analyse Environnementale du Québec, Ministère de l'Environnement du Québec, Québec, QC, Canada.

Chen, C., Yang, S., Guo, Y., Sun, C., Gu, C. and Xu, B. (2009) Photolytic destruction of endocrine disruptor atrazine in aqueous solution under UV irradiation: Products and pathways. Journal of Hazardous Materials 172(2–3), 675-684.

Chien, Y.-Y., Kim, E.-G. and Bleam, W.F. (1997) Paramagnetic Relaxation of Atrazine Solubilized by Humic Micellar Solutions. Environmental Science & Technology 31(11), 3204-3208.

Comninellis, C. (1994) Electrocatalysis in the electrochemical conversion/combustion of organic pollutants for waste water treatment. Electrochimica Acta 39(11–12), 1857-1862.

Criquet, J. and Leitner, N.K.V. (2009) Degradation of acetic acid with sulfate radical generated by persulfate ions photolysis. Chemosphere 77(2), 194-200.

De Laat, J. and Gallard, H. (1999) Catalytic Decomposition of Hydrogen Peroxide by Fe(III) in Homogeneous Aqueous Solution: Mechanism and Kinetic Modeling. Environmental Science & Technology 33(16), 2726-2732.

de Melo, B.A.G., Motta, F.L. and Santana, M.H.A. (2016) Humic acids: Structural properties and multiple functionalities for novel technological developments. Materials Science and Engineering: C 62, 967-974.

DeLorenzo, M.E., Scott, G.I. and Ross, P.E. (2001) Toxicity of pesticides to aquatic microorganisms: A review. Environmental Toxicology and Chemistry 20(1), 84-98.

Ding, X., Wang, S., Shen, W., Mu, Y., Wang, L., Chen, H. and Zhang, L. (2017) Fe@Fe2O3 promoted electrochemical mineralization of atrazine via a triazinon ring opening mechanism. Water Research 112, 9-18.

Drogui, P. and Lafrance, P. (2012) Farming for Food and Water Security. Lichtfouse, E. (ed), pp. 23-55, Springer, Allemagne.

Fukushima, M. and Tatsumi, K. (2001) Degradation Pathways of Pentachlorophenol by Photo-Fenton Systems in the Presence of Iron(III), Humic Acid, and Hydrogen Peroxide. Environmental Science & Technology 35(9), 1771-1778.

Garza-Campos, B.R., Guzmán-Mar, J.L., Reyes, L.H., Brillas, E., Hernández-Ramírez, A. and Ruiz-Ruiz, E.J. (2014) Coupling of solar photoelectro-Fenton with a BDD anode and solar heterogeneous photocatalysis for the mineralization of the herbicide atrazine. Chemosphere 97(0), 26-33.

Giroux, I. and Pelletier, L. (2012) Présence de pesticides dans l'eau au Québec : bilan dans quatre cours d'eau de zones en culture de maïs et de soya en 2008, 2009 et 2010, Québec, Ministère du Développement durable, de l'Environnement et des Parcs.

Giroux, I., Roy, N. and Lamontagne, C. (2010) Présence de Pesticides dans l'Eau Souterraine en Milieu Agricole : Étude Pilote du Bassin Versant de la Rivière Châteauguay. Canadian Water Resources Journal 35(4), 527-542.

Guetzloff, T.F. and Rice, J.A. (1994) Does humic acid form a micelle? Science of the Total Environment 152(1), 31-35.

Hayes, T.B., Khoury, V., Narayan, A., Nazir, M., Park, A., Brown, T., Adame, L., Chan, E., Buchholz, D., Stueve, T. and Gallipeau, S. (2010) Atrazine induces complete feminization and chemical castration in male African clawed frogs (Xenopus laevis). Proceedings of the National Academy of Sciences, USA 107(10), 4612-4617.

Herrmann, H. (2007) On the photolysis of simple anions and neutral molecules as sources of O-/OH, SOx- and Cl in aqueous solution. Physical Chemistry Chemical Physics 9(30), 3935-3964.

Hildebrandt, A., Guillamón, M., Lacorte, S., Tauler, R. and Barceló, D. (2008) Impact of pesticides used in agriculture and vineyards to surface and groundwater quality (North Spain). Water Research 42(13), 3315-3326.

Irmak, S., Yavuz, H.I. and Erbatur, O. (2006) Degradation of 4-chloro-2-methylphenol in aqueous solution by electro-Fenton and photoelectro-Fenton processes. Applied Catalysis B: Environmental 63(3–4), 243-248.

Khataee, A.R., Safarpour, M., Naseri, A. and Zarei, M. (2012) Photoelectro-Fenton/nanophotocatalysis decolorization of three textile dyes mixture: Response surface modeling and multivariate calibration procedure for simultaneous determination. Journal of Electroanalytical Chemistry 672, 53-62.

Komtchou, S., Dirany, A., Drogui, P. and Bermond, A. (2015) Removal of carbamazepine from spiked municipal wastewater using electro-Fenton process. Environmental Science and Pollution Research, 1-13.

Komtchou, S., Drogui, P., Dirany, A. and Lafrance, P. (2016a) Application des procédés d’oxydation avancée pour le traitement des eaux contaminées par les pesticides – revue de littérature. Journal of Water Science 29(3), 231-262.

Komtchou, S., Dirany, A., Drogui, P., Delegan, N., El Khakani, M.A., Robert, D. and Lafrance, P. (2016b) Degradation of atrazine in aqueous solution with electrophotocatalytic process using TiO2−x photoanode. Chemosphere 157, 79-88.

Koprivnikar, J. (2010) Interactions of environmental stressors impact survival and development of parasitized larval amphibians. Ecological Applications 20(8), 2263-2272.

Lee, C. and Yoon, J. (2004) Temperature dependence of hydroxyl radical formation in the hν/Fe3+/H2O2 and Fe3+/H2O2 systems. Chemosphere 56(10), 923-934.

Martin-Neto, L., Traghetta, D.G., Vaz, C.M.P., Crestana, S. and Sposito, G. (2001) On the Interaction Mechanisms of Atrazine and Hydroxyatrazine with Humic Substances. Journal of Environmental Quality 30(2), 520-525.

Masomboon, N., Ratanatamskul, C. and Lu, M.-C. (2010) Mineralization of 2,6-dimethylaniline by photoelectro-Fenton process. Applied Catalysis A 384(1–2), 128-135.

Neuman-Lee, L.A. and Janzen, F.J. (2011) Atrazine Exposure Impacts Behavior and Survivorship of Neonatal Turtles. Herpetologica 67(1), 23-31.

Oturan, N., Brillas, E. and Oturan, M. (2012) Unprecedented total mineralization of atrazine and cyanuric acid by anodic oxidation and electro-Fenton with a boron-doped diamond anode. Environmental Chemistry Letters 10(2), 165-170.

Ou, X., Quan, X., Chen, S., Zhao, H. and Zhang, Y. (2007) Atrazine Photodegradation in Aqueous Solution Induced by Interaction of Humic Acids and Iron: Photoformation of Iron(II) and Hydrogen Peroxide. Journal of Agricultural and Food Chemistry 55(21), 8650-8656.

Panizza, M. and Cerisola, G. (2009) Direct and mediated anodic oxidation of organic pollutants. Chemical Reviews 109(12), 6541-6569.

Prosen, H. and Zupančič-Kralj, L. (2005) Evaluation of photolysis and hydrolysis of atrazine and its first degradation products in the presence of humic acids. Environmental Pollution 133(3), 517-529.

Reilly, T.J., Smalling, K.L., Orlando, J.L. and Kuivila, K.M. (2012) Occurrence of boscalid and other selected fungicides in surface water and groundwater in three targeted use areas in the United States. Chemosphere 89(3), 228-234.

Sigler, P.B. and Masters, B.J. (1957) The Hydrogen Peroxide-induced Ce*(III)-Ce(IV) Exchange System1. Journal of the American Chemical Society 79(24), 6353-6357.

Sirés, I., Brillas, E., Oturan, M., Rodrigo, M. and Panizza, M. (2014) Electrochemical advanced oxidation processes: today and tomorrow. A review. Environmental Science and Pollution Research 21(14), 8336-8367.

Solomon, K.R., Baker, D.B., Richards, R.P., Dixon, K.R., Klaine, S.J., La Point, T.W., Kendall, R.J., Weisskopf, C.P., Giddings, J.M., Giesy, J.P., Hall, L.W. and Williams, W.M. (1996) Ecological risk assessment of atrazine in North American surface waters. Environmental Toxicology and Chemistry 15(1), 31-76.

Sum, O.S.N., Feng, J., Hub, X. and Yue, P.L. (2005) Photo-assisted fenton mineralization of an azo-dye acid black 1 using a modified laponite clay-based Fe nanocomposite as a heterogeneous catalyst. Topics in Catalysis 33(1), 233-242.

Torrents, A., Anderson, B.G., Bilboulian, S., Johnson, W.E. and Hapeman, C.J. (1997) Atrazine Photolysis: Mechanistic Investigations of Direct and Nitrate-Mediated Hydroxy Radical Processes and the Influence of Dissolved Organic Carbon from the Chesapeake Bay. Environmental Science & Technology 31(5), 1476-1482.

Trentacoste, S.V., Friedmann, A.S., Youker, R.T., Breckenridge, C.B. and Zirkin, B.R. (2001) Atrazine Effects on Testosterone Levels and Androgen-Dependent Reproductive Organs in Peripubertal Male Rats. Journal of Andrology 22(1), 142-148.

von Wandruszka, R. (1998) The micellar model of humic acid: evidence from pyrene fluorescence measurements. Soil Science 163(12), 921-930.

Table 1 Current density effect to the removal of ATZ after 15 min of treatment

d (mA cm^{-2})	Removal of ATZ (%)	k_{app} (min^{-1})	Half-life (min)	EC (kWh m^{-3})
1	38.12	0.04	17.33	1.43
4.5	56.85	0.09	7.70	31.88
9.1	68.18	0.13	5.33	43.85
18.2	99.57	0.36	1.93	55

Table 2 Chemicals analysis of the water of the river

Compound	**Mean (mg L^{-1})**	**Standard deviation (mg L^{-1})**
Cl^-	9.58	0.14
SO_4^{2-}	9.32	0.17
NO_3^-	2.24	0.03
Ca^{2+}	19.63	0.14
Na^+	4.50	0.07
Mg^{2+}	3.86	0.04
K^+	2.51	0.06
Fe_{total}	0.66	0.06
Al	0.64	0.07
Si	3.39	0.14
S	3.34	0.06
P_{total}	0.05	0.01

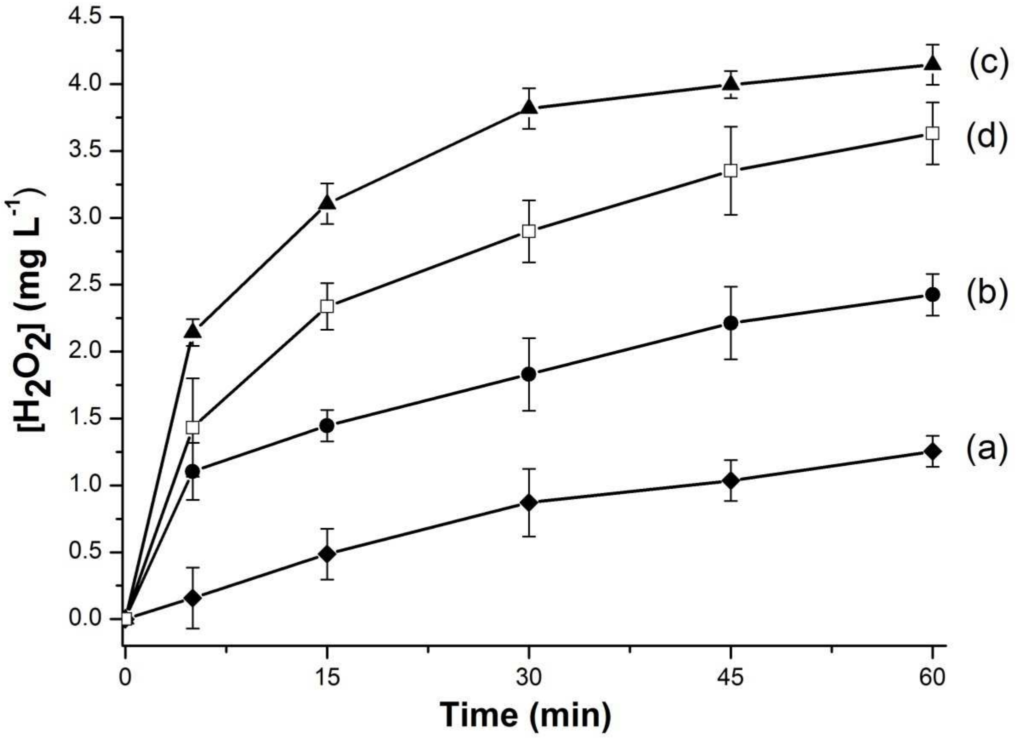

Fig. 1 Production of H_2O_2 during the electrolysis of 5.0 L containing 0.03 M of Na_2SO_4 at pH 3.0 with different current density: (a) 2 mA cm^{-2}, (b) 9.1 mA cm^{-2}, (c) 18.2 mA cm^{-2} and (d) 18.2 mA cm^{-2} under UV light at 254 nm. The bars represent standard deviations.

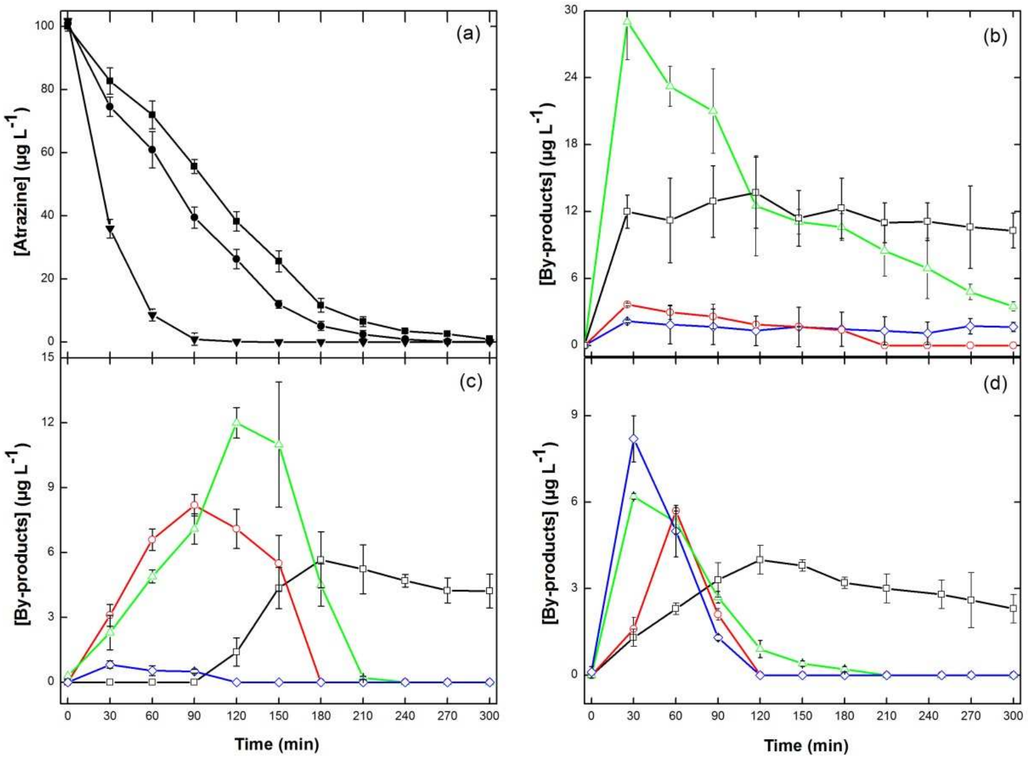

Fig. 2 Removal of atrazine (100 µg L^{-1}) in solution (5 L) at pH 3.0 with 2 mA cm^{-2} using the electrochemical advanced oxidation processes (a): (■) AO-H_2O_2, (●) EF and (▼) PEF. Evolution of by-products of atrazine : (□) DEDIA, (○) DIA, (Δ) DEA and (◊) ATZ-OH during electrolysis by AO-H_2O_2 (b), EF (c) and PEF (d). The bars represent standard deviations.

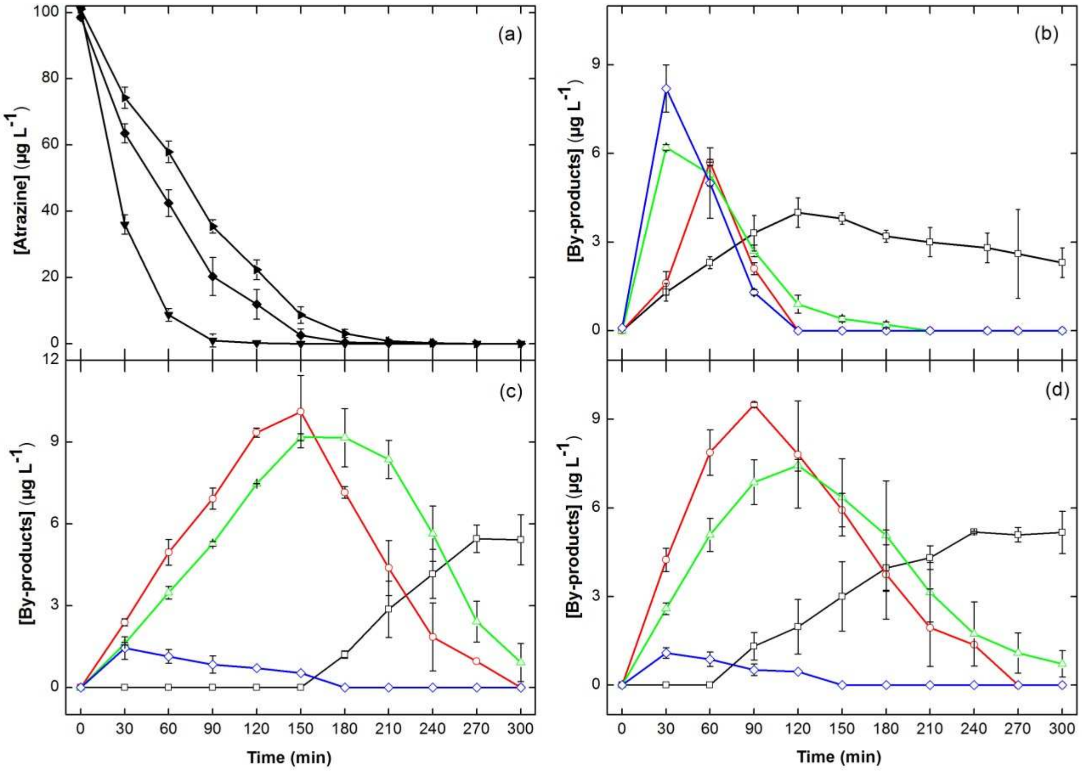

Fig. 3 Removal of atrazine (100 µg L^{-1}) in solution (5 L) using PEF process at pH 3.0 with different wavelength lights (a): (▼) 254 nm, (►) 365 nm and (♦) 567 nm. Evolution of by-products of atrazine : (□) DEDIA, (○) DIA, (Δ) DEA and (◊) ATZ-OH during electrolysis using 254 nm (b), 365 nm (c) and 567 nm (d). The bars represent standard deviations.

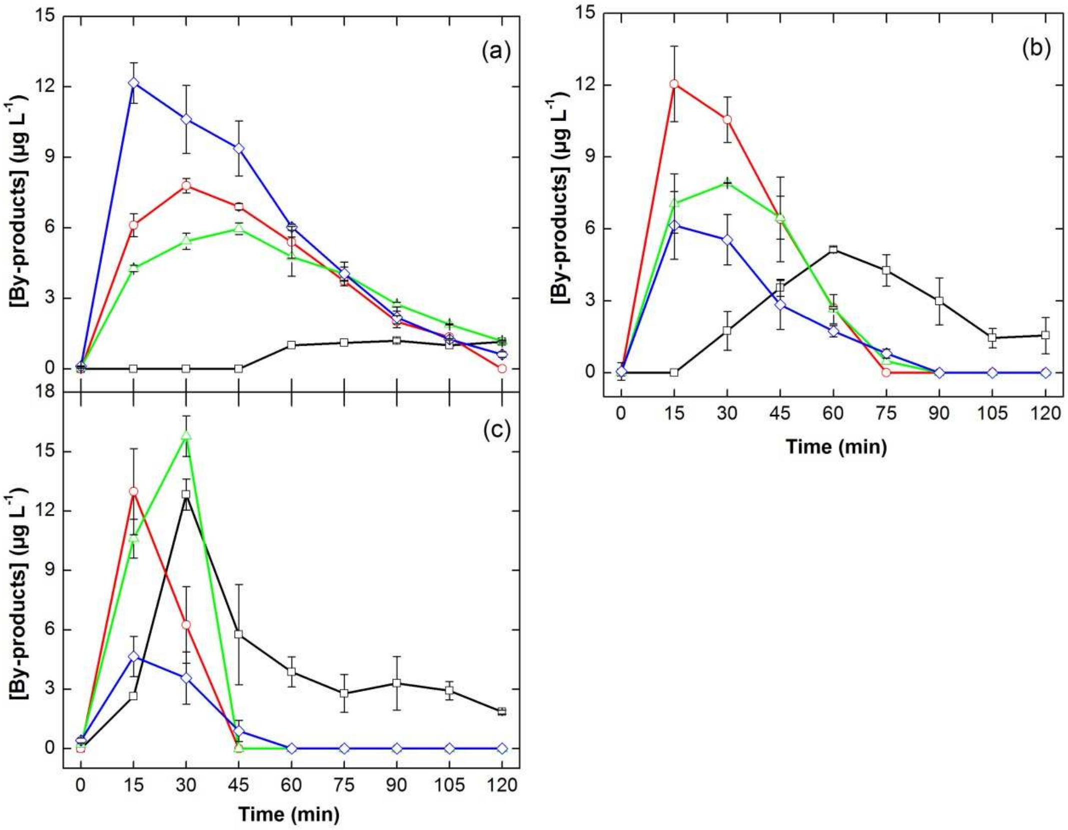

Fig. 4 Evolution of by-products of atrazine: (□) DEDIA, (○) DIA, (∆) DEA and (◊) ATZ-OH during PEF process with 1 mA cm^{-2} (a), 4.5 mA cm^{-2} (b) and 9.1 mA cm^{-2} (c) by PEF process using 254 nm. The bars represent standard deviations.

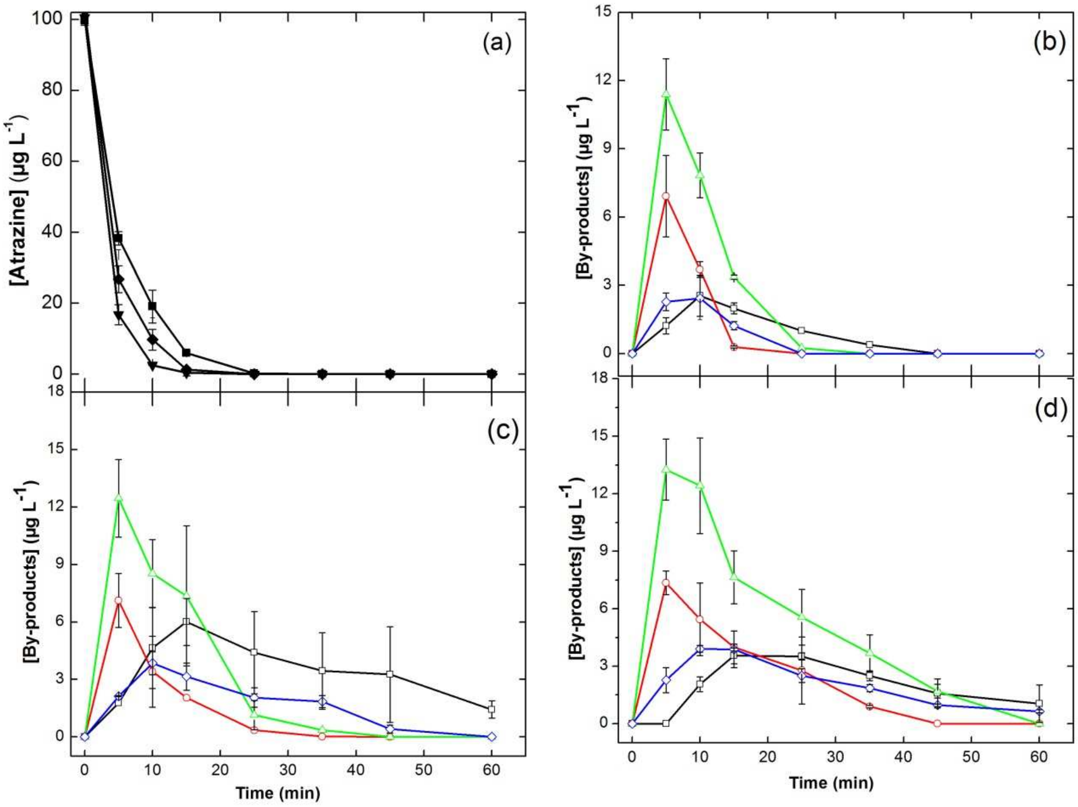

Fig. 5 Removal of atrazine (100 µg L^{-1}) in solution (5 L) at pH 3.0 without humic acids (▼), with 5.0 mg L^{-1} (♦) and with 10.0 mg L^{-1} (■) of humic acids at 18.2 mA cm^{-2} by PEF process using 254 nm. Evolution of by-products of atrazine : (□) DEDIA, (○) DIA, (Δ) DEA and (◊) ATZ-OH during PEF process without humic acids (b), with 5.0 mg L^{-1} (c) and 10.0 mg L^{-1} of humic acids (d). The bars represent standard deviations.

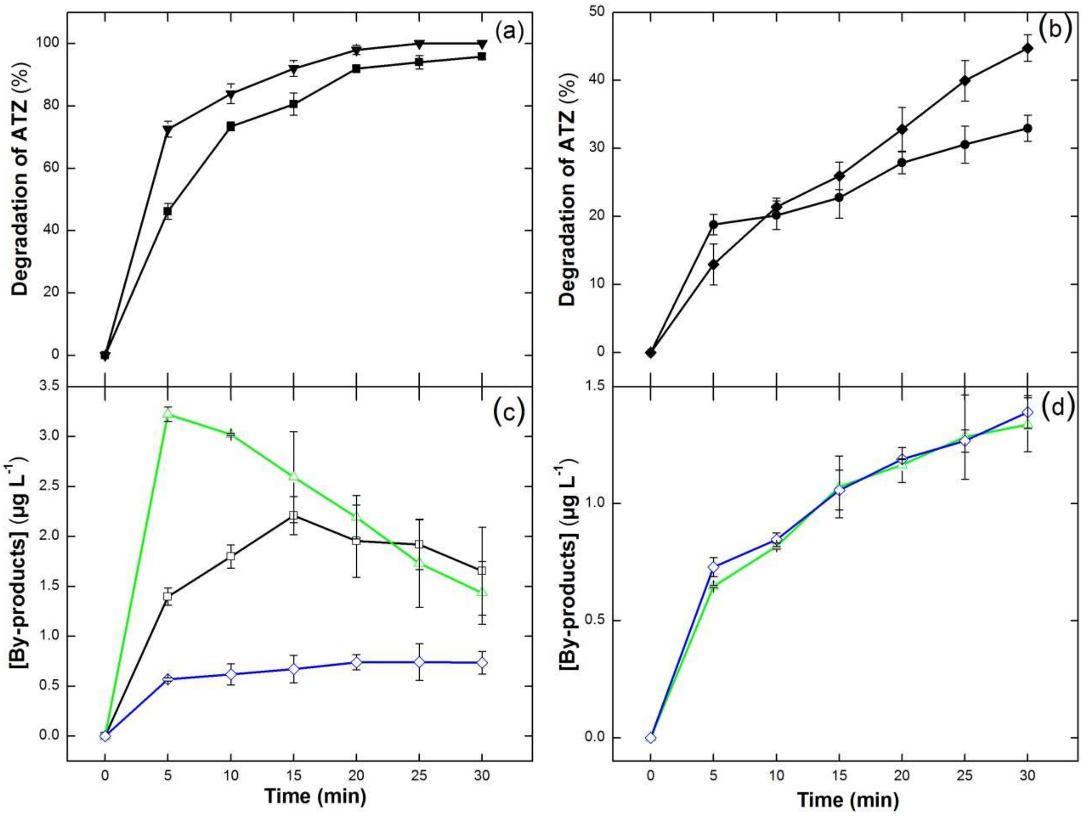

Fig. 6 Removal of atrazine (10 μg L^{-1}) in river water (5 L) using 18.2 mA cm^{-2} at pH 3 in plot (a), (▼) with 0.1 mM of iron and (■) without iron adjustment. At pH 6.7 in plot (b), (●) with 0.1 mM of iron and (♦) without iron adjustment. In plot (c) evolution of by-products of atrazine: (□) DEDIA, (Δ) DEA and (◊) ATZ-OH during PEF process with 0.1 mM of iron at pH 3.1. In plot (d) evolution of by-products of atrazine: (Δ) DEA and (◊) ATZ-OH during PEF process without iron adjustment at pH 3.1. The bars represent standard deviations.

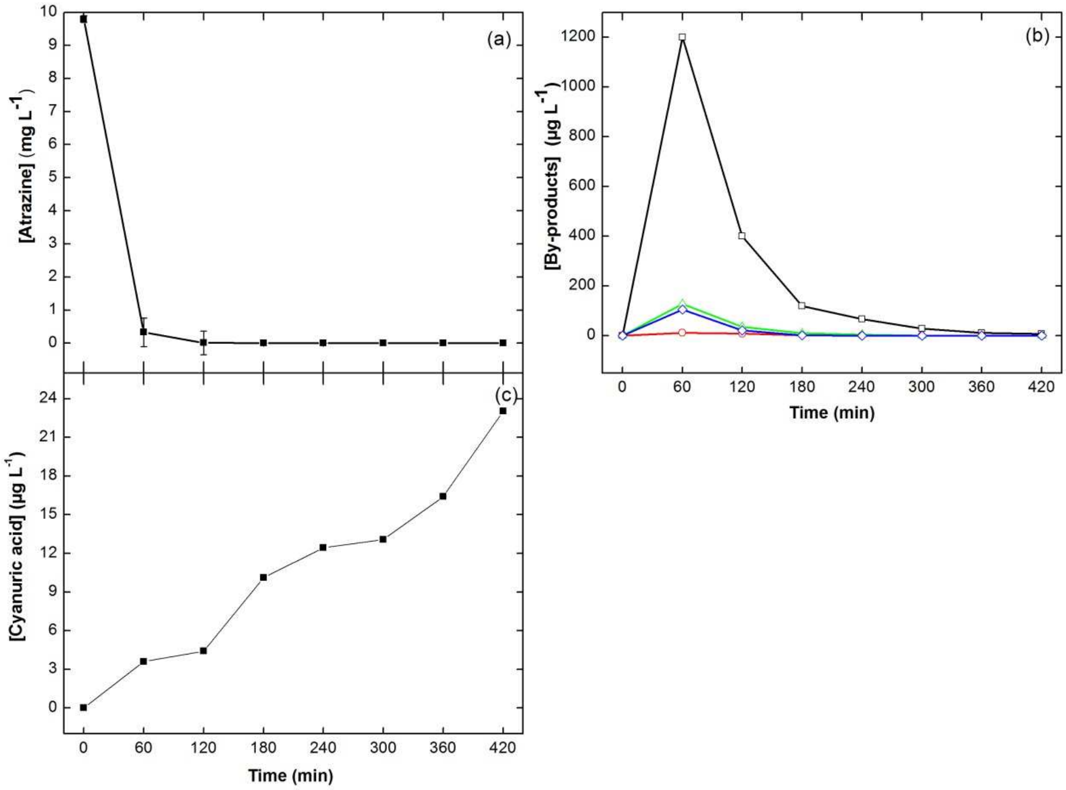

Fig. 7 Degradation of atrazine (10 mg L^{-1}) in river water (5 L) using 18.2 mA cm^{-2} at pH 3.1 (a). Evolution of by-products of atrazine: (□) DEDIA, (○) DIA, (Δ) DEA and (◊) ATZ-OH during PEF process (b). Evolution of cyanuric acid during PEF process (c). The bars represent standard deviations.

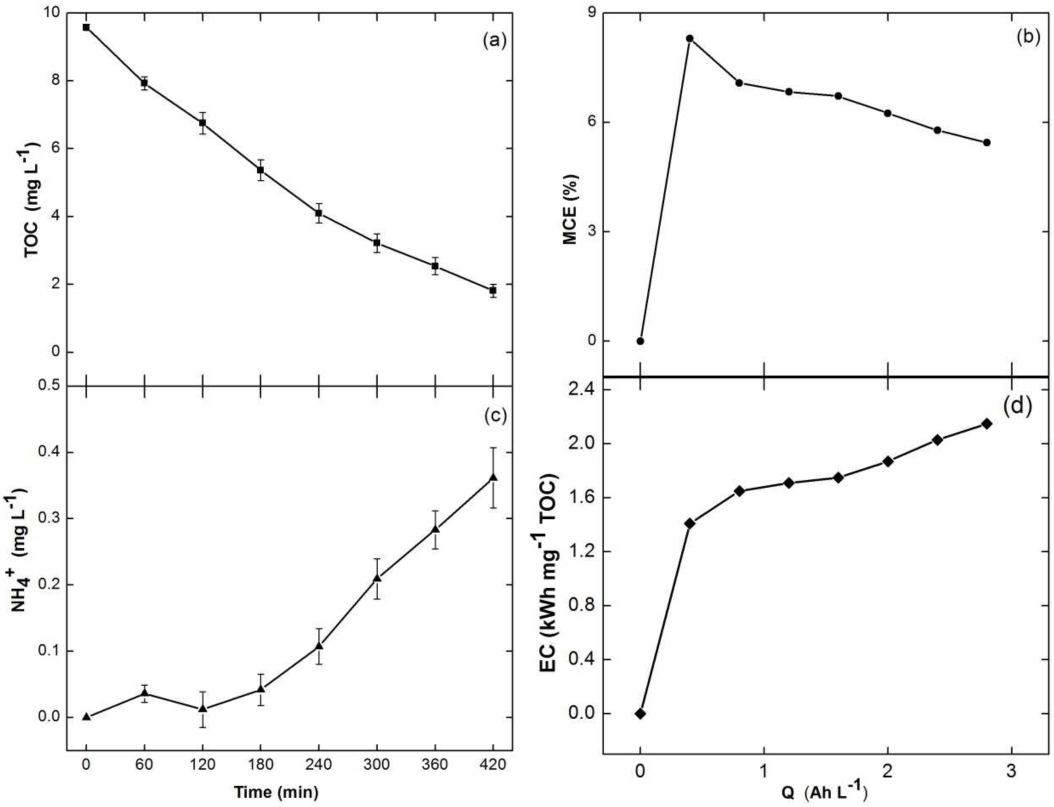

Fig. 8 Total organic carbon abatement (a), evolution of mineralization current efficiency (b), NH_4^+ (c) and energy consumption (d) during the electrolysis of river water effluent (5 L) using 18.2 mA cm^{-2} at pH 3.1. The bars represent standard deviations.

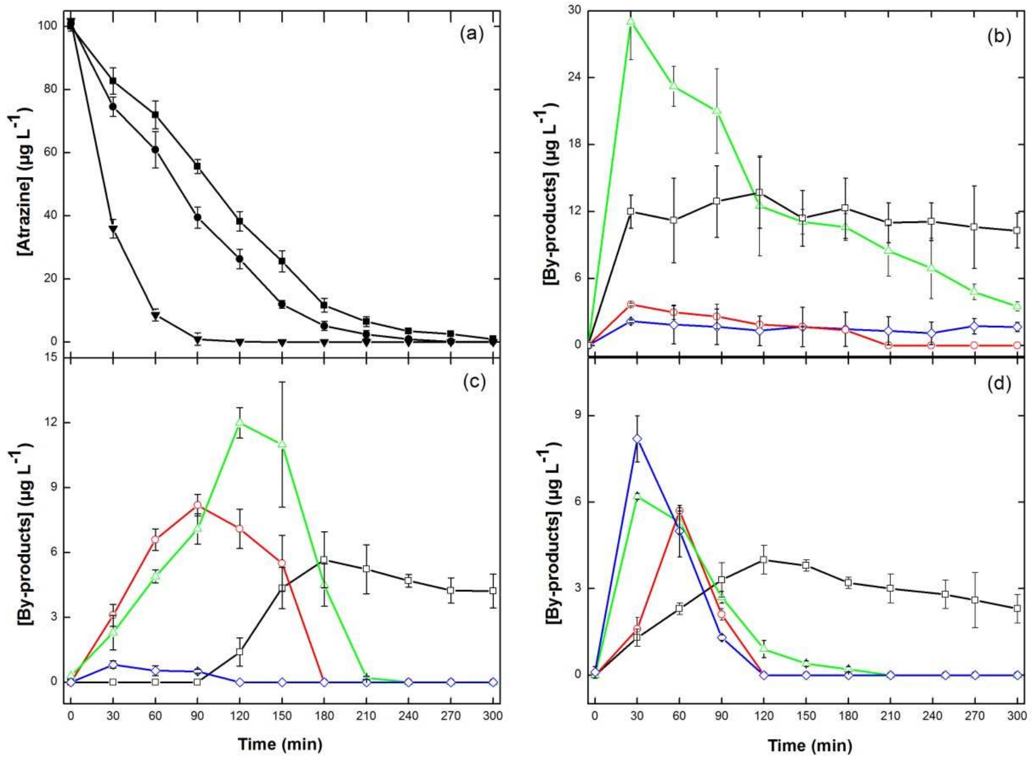

Fig. 2 Removal of atrazine (100 µg L^{-1}) in solution (5 L) at pH 3.0 with 2 mA cm^{-2} using the electrochemical advanced oxidation processes (a): (■) AO-H_2O_2, (●) EF and (▼) PEF. Evolution of by-products of atrazine : (□) DEDIA, (○) DIA, (Δ) DEA and (◊) ATZ-OH during electrolysis by AO-H_2O_2 (b), EF (c) and PEF (d). The bars represent standard deviations.

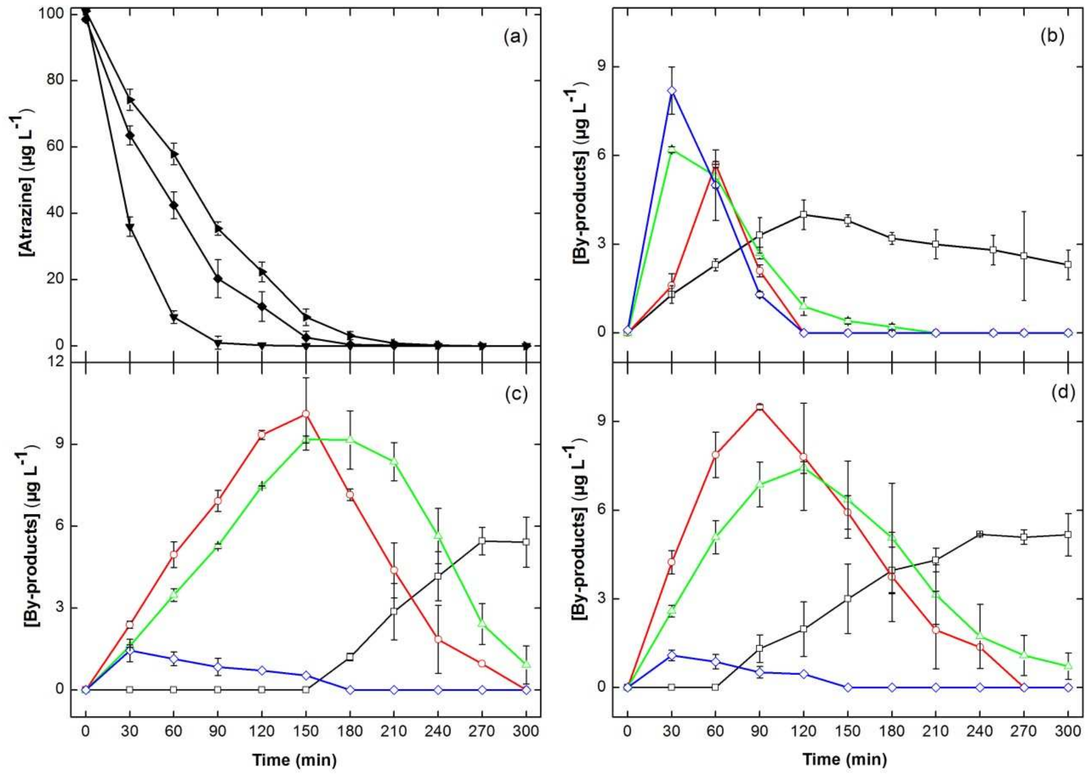

Fig. 3 Removal of atrazine (100 μg L^{-1}) in solution (5 L) using PEF process at pH 3.0 with different wavelength lights (a): (▼) 254 nm, (►) 365 nm and (♦) 567 nm. Evolution of by-products of atrazine : (□) DEDIA, (○) DIA, (Δ) DEA and (◊) ATZ-OH during electrolysis using 254 nm (b), 365 nm (c) and 567 nm (d). The bars represent standard deviations

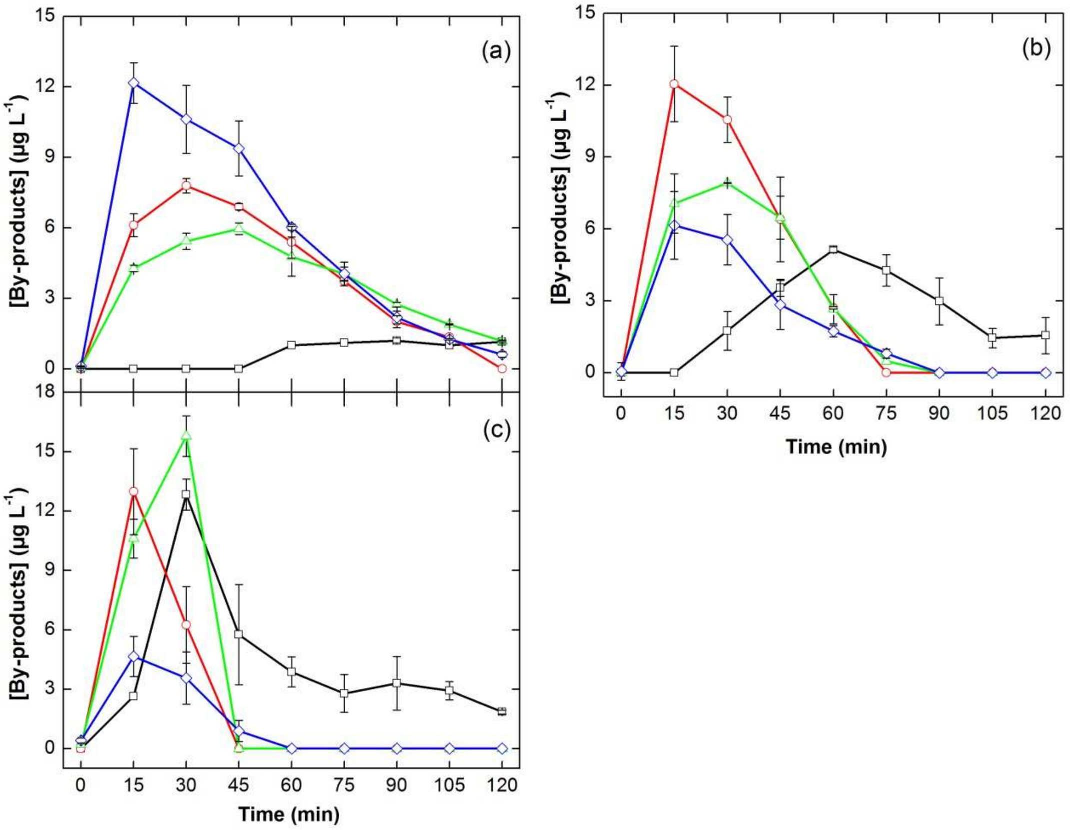

Fig. 4 Evolution of by-products of atrazine: (□) DEDIA, (○) DIA, (Δ) DEA and (◊) ATZ-OH during PEF process with 1 mA cm^{-2} (a), 4.5 mA cm^{-2} (b) and 9.1 mA cm^{-2} (c) by PEF process using 254 nm. The bars represent standard deviations

.

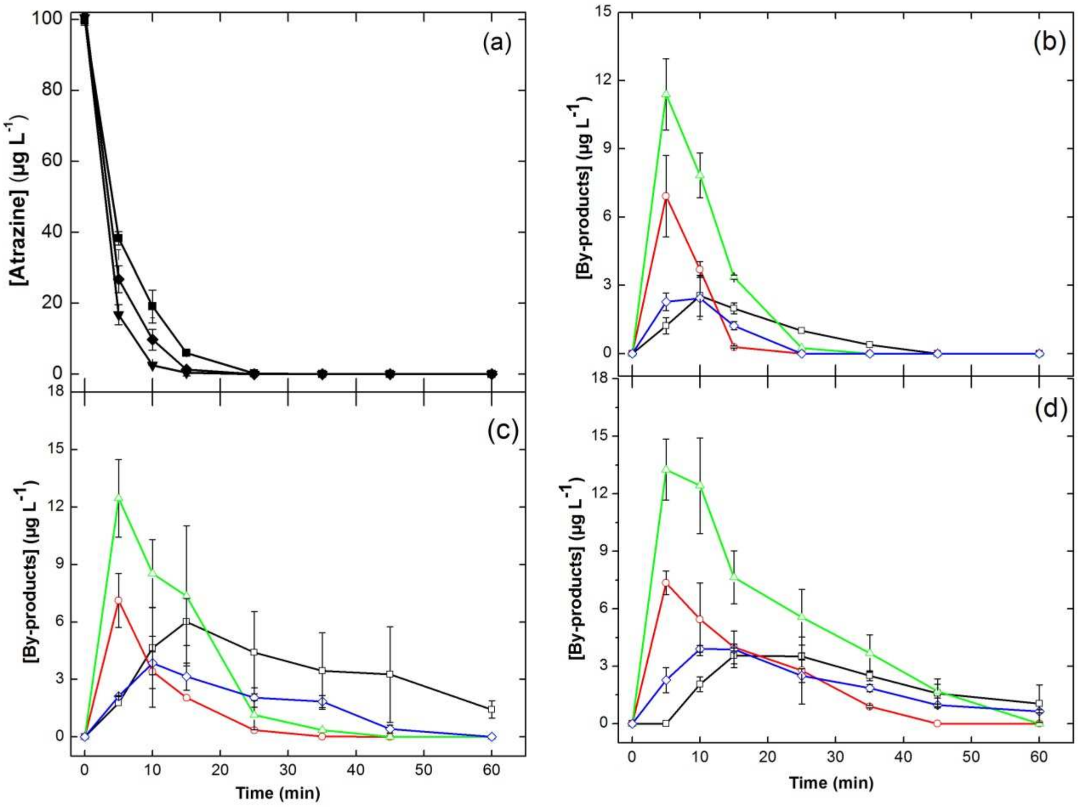

Fig. 5 Removal of atrazine (100 µg L^{-1}) in solution (5 L) at pH 3.0 without humic acids (▼), with 5.0 mg L^{-1} (♦) and with 10.0 mg L^{-1} (■) of humic acids at 18.2 mA cm^{-2} by PEF process using 254 nm. Evolution of by-products of atrazine : (□) DEDIA, (○) DIA, (Δ) DEA and (◊) ATZ-OH during PEF process without humic acids (b), with 5.0 mg L^{-1} (c) and 10.0 mg L^{-1} of humic acids (d). The bars represent standard deviations.

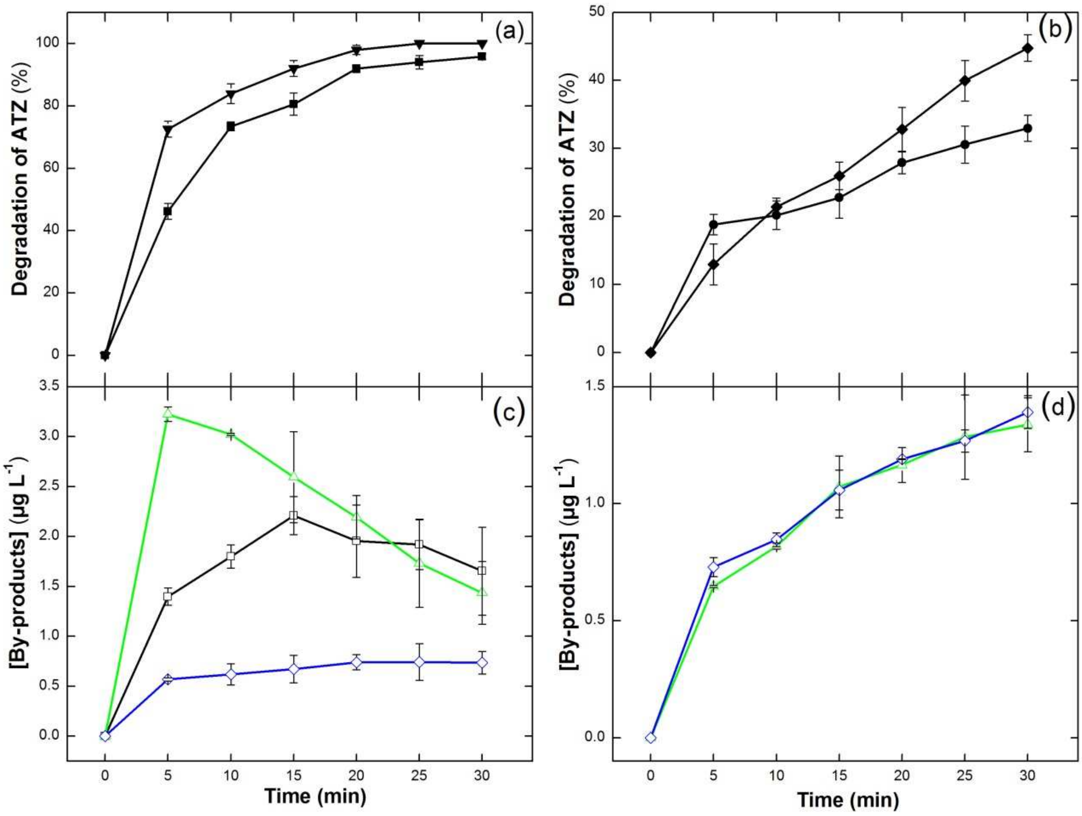

Fig. 6 Removal of atrazine (10 µg L^{-1}) in river water (5 L) using 18.2 mA cm^{-2} at pH 3 in plot (a), (▼) with 0.1 mM of iron and (■) without iron adjustment. At pH 6.7 in plot (b), (●) with 0.1 mM of iron and (♦) without iron adjustment. In plot (c) evolution of by-products of atrazine: (□) DEDIA, (Δ) DEA and (◊) ATZ-OH during PEF process with 0.1 mM of iron at pH 3.1. In plot (d) evolution of by-products of atrazine: (Δ) DEA and (◊) ATZ-OH during PEF process without iron adjustment at pH 3.1. The bars represent standard deviations.

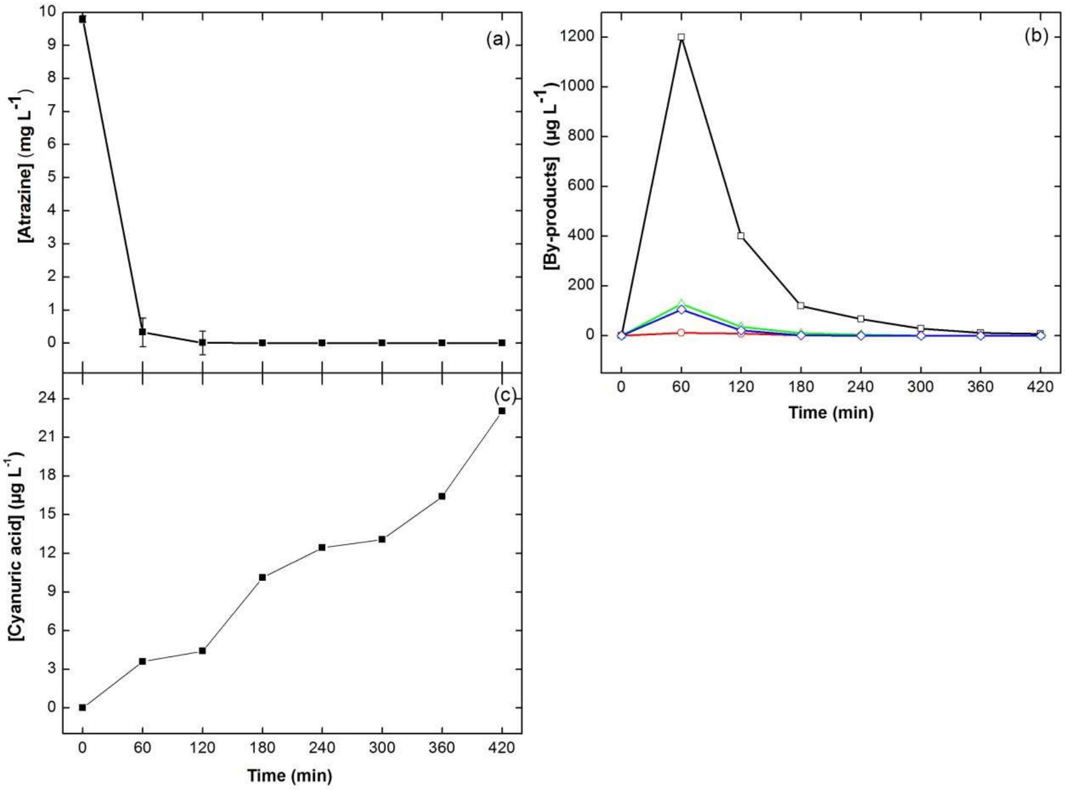

Fig. 7 Degradation of atrazine (10 mg L^{-1}) in river water (5 L) using 18.2 mA cm^{-2} at pH 3.1 (a). Evolution of by-products of atrazine: (□) DEDIA, (○) DIA, (∆) DEA and (◊) ATZ-OH during PEF process (b). Evolution of cyanuric acid during PEF process (c). The bars represent standard deviations.

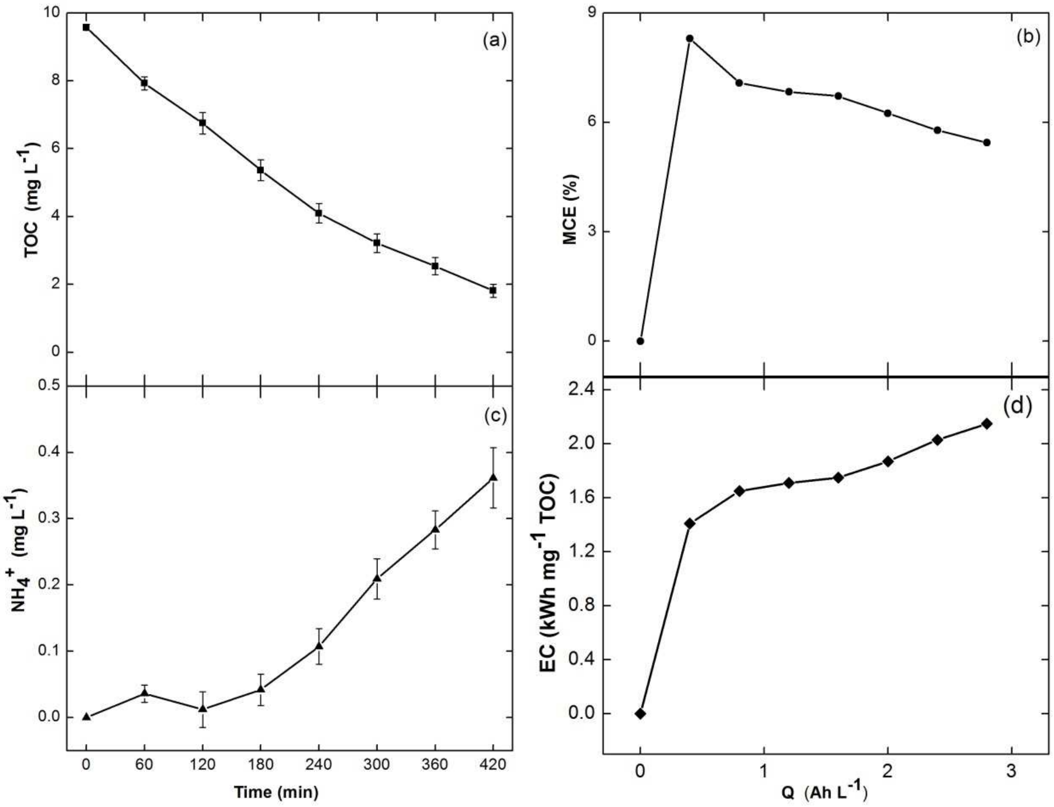

Fig. 8 Total organic carbon abatement (a), evolution of mineralization current efficiency (b), NH_4^+ (c) and energy consumption (d) during the electrolysis of river water effluent (5 L) using 18.2 mA cm^{-2} at pH 3.1. The bars represent standard deviations.